Materials Advances

ROYAL SOCIETY OF CHEMISTRY

REVIEW

View Article Online
View Journal | View Issue

Cite this: *Mater. Adv.*, 2022, 3, 2971

Magnetic nanocarriers adorned on graphene: promising contrast-enhancing agents with state-of-the-art performance in magnetic resonance imaging (MRI) and theranostics

Shikha Gulati, *[a] Mansi,[a] Sneha Vijayan,[a] Sanjay Kumar,[a] Varnika Agarwal,[b] Bharath Harikumar[a] and Rajender S. Varma *[c]

Received 14th November 2021,
Accepted 14th February 2022

DOI: 10.1039/d1ma01071a

rsc.li/materials-advances

Magnetic resonance imaging (MRI) is an effectual imaging technique for medical diagnosis, its non-invasive nature being a noteworthy attribute, in which magnetic contrast agents are employed to improve sensitivity and accuracy. Graphene exhibits excellent mechanical and physicochemical properties, and notable biocompatibility. In the quest for superior contrast agents with low toxicity, improved chemical stability, and remarkable functionalization potential, graphene-based magnetic nanocarriers have piqued the interest of researchers. Graphene and its derivatives function as nanocarriers or platforms onto which magnetic nanoparticles are anchored, due to its high specific surface area which prevents the uncontrolled aggregation of nanoparticles and thus provides extra stability while significantly increasing the MRI efficiency. Herein, the recent trends in the application of graphene-based magnetic nanocarriers as potential contrast agents in MRI are deliberated with detailed discussion on the methods of preparation, classification, and significant features, including theranostic applications. The cytotoxicity and biocompatibility of magnetic nanocarrier adorned graphene are also analyzed and highlighted along with their future outlook.

[a] *Department of Chemistry, Sri Venkateswara College, University of Delhi, Delhi-110021, India. E-mail: shikha2gulati@gmail.com*
[b] *Department of Materials, University of Oxford, UK*
[c] *Regional Centre of Advanced Technologies and Materials, Czech Advanced Technology and Research Institute, Palacký University in Olomouc, Šlechtitelů 27, 783 71 Olomouc, Czech Republic. E-mail: Varma.Rajender@epa.gov*

1. Introduction

Magnetic resonance imaging (MRI) is one of the most commonly used imaging techniques in diagnostics, with a broad spectrum of biomedical applications including high-quality 3D

Shikha Gulati

Dr Shikha Gulati (MSc, PhD) is working as an assistant professor of chemistry at Sri Venkateswara College, University of Delhi. She has expertise in inorganic chemistry, nano-materials, green chemistry, catalysis, and analytical chemistry. Dr Shikha has authored several research papers in reputable international journals and written numerous books as well as chapters in diverse books which attest to her research aptitude, and good writing skills. Her books are referred to in many Universities across India for different undergraduate courses. Dr Gulati has also been awarded the Young Researcher Award 2020 for her work in the field of nanotechnology.

Mansi

Mansi was born in Haryana, India, in 2002. Currently, she is pursuing a bachelor's degree in Chemistry from Sri Venkateswara College, University of Delhi. She aspires to pursue research in the field of medicinal chemistry. Her research interests also include synthesis and applications of nanomaterials, green chemistry, drug synthesis, and theranostics.

imaging of tissues for disease detection, diagnosis, and monitoring of treatment. MRI uses strong magnetic fields and radio waves to generate detailed computerized images of the internal body structures. Being a non-invasive technique that does not involve radiations, it is regarded as one of the most powerful diagnostic tools available today.[1–5] MRI contrast agents (CAs) are used to shorten the relaxation time of nuclei within body tissues, thereby improving the visibility of internal body structures. Gadolinium, which is a conventional MRI contrast agent, is toxic and is found to have a general depressant activity on all body systems. Furthermore, there is a chance that free Gd^{3+} ions would be released from the chelated Gd CAs which would be neurotoxic and would affect the cardiovascular system, with the potential to inhibit the calcium channels in the body.[6] Therefore, it is necessary to couple gadolinium with some other substances to eliminate/exterminate its toxicity

Sneha Vijayan

Sneha Vijayan was born in Kerala, India, in 2002. Currently, she is pursuing a BSc (Honours) degree in Chemistry from Sri Venkateswara College, University of Delhi. Her research interests are focused in materials science, nanotechnology, biomedicine, and green chemistry. She also has keen interest in cancer theranostics using nanotechnology.

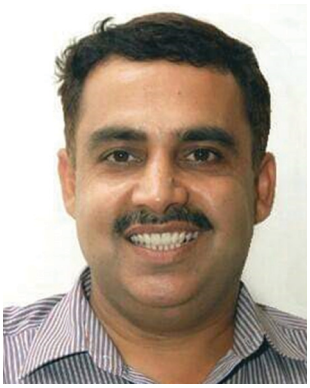

Sanjay Kumar

Prof. Sanjay Kumar has been working as a professor in the Department of Chemistry, Sri Venkateswara College, the University of Delhi since 2000. He undertook his PhD in the field of molecular spectroscopy from the University of Delhi in 1998. He has also worked as a post-doctoral fellow at IGIB, New Delhi in the field of molecular immunology. Currently, he is focusing on the field of nanotechnology and cancer research. He has authored several research papers in reputed international journals and written several books on chemistry and environmental sciences.

Varnika Agarwal

Varnika Agarwal is doing her DPhil in Materials Science from the University of Oxford. She is a member of Linacre College, Oxford. Her current research focuses on solid-state batteries for electric vehicles. She has worked on graphene quantum dots for solar cells. She completed her Bachelor's degree in Chemistry from Sri Venkateswara College, University of Delhi. Her research interests include nanomaterials, energy storage, green chemistry, electro chemistry, and the fabrication of composite alloys.

Rajender S. Varma

Prof. Varma completed his PhD from Delhi University in 1976. After postdoctoral research at Robert Robinson Laboratories, Liverpool, UK, he was a faculty member at the Baylor College of Medicine and Sam Houston State University prior to joining the Sustainable Technology Division at the US Environmental Protection Agency in 1999 with an appointment at the Regional Centre of Advanced Technologies and Materials, Palacky University at Olomouc, the Czech Republic from 2014. He has over 48 years of research experience in the management of multidisciplinary technical programs ranging from natural products chemistry to the development of more environmentally friendly synthetic methods using microwaves, ultrasound, etc. Lately, he has focused on greener approaches to the assembly of nanomaterials and sustainable applications of magnetically retrievable nanocatalysts in benign media. He is a member of the editorial advisory board of several international journals, has published over 800 scientific papers, has been awarded 17 US Patents, and has authored 8 books, 28 book chapters, and 3 encyclopedia contributions with more than 54 500 citations.

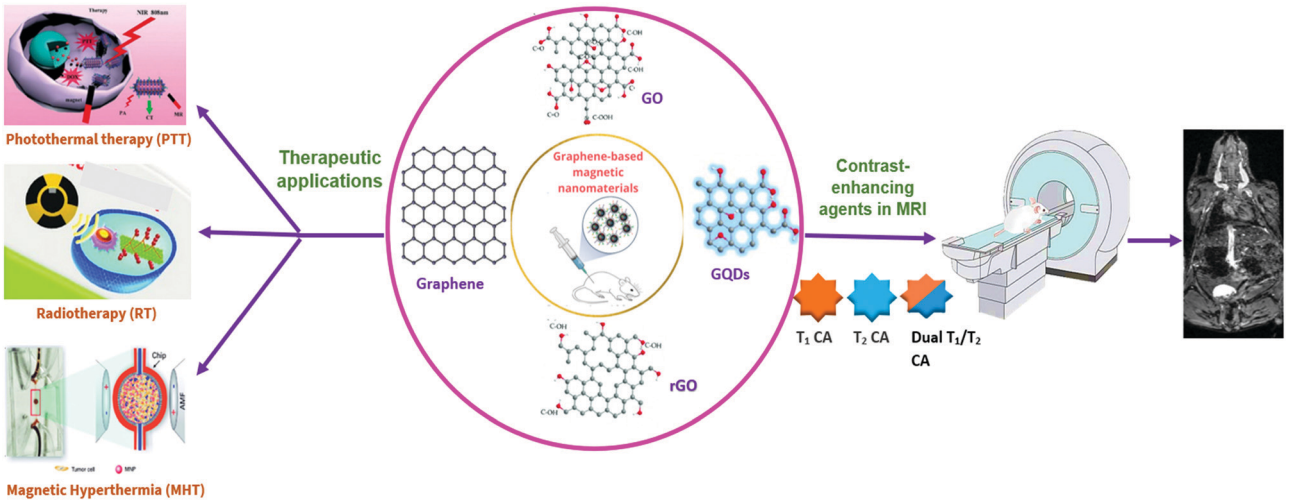

Fig. 1 Schematic representation of graphene-based magnetic nanomaterials in MRI and therapeutic applications.

while retaining the properties of a good MRI contrast agent or to seek out a safer and more efficacious alternative to gadolinium-based contrast agents.

Graphene, often dubbed as the 'wonder material', has garnered tremendous attention in the field of nanomaterial research due to its unique set of properties. Graphene-based nanomaterials have a wide range of diagnostics applications, one of them being contrast agents in MRI, and therapeutic applications (Fig. 1). These ultra-light nanoparticles have various desirable properties such as a high surface area, excellent electrical conductivity and thermal conductivity, chemical inertness, and mechanical strength. Because of these favorable properties of graphene and graphene derivatives, they are used in the field of biomedicine in various ways such as drug- and gene-delivery agents, and multimodal imaging probes,[7] as well as in the detection (at early stages) and treatment of cancer.[8–12] The salient advantageous features that graphene-based nanomaterials possess over other carbon-based materials, comprise a large surface area, better solubility, and ease of modification by various functional groups which makes them an excellent choice for biomedical applications. Among graphene-based nanomaterials, graphene oxide (GO) is one of the most promising materials for biomedical use.[13] In comparison to fullerenes and carbon nanotubes, which have been extensively used as nanoplatforms for designing MRI contrast agents, GO shows remarkable advantages. These include its low cost and improved water dispersibility owing to the abundance of hydrophilic oxygen-containing groups in its structure.[14] Materials like SPIONs (superparamagnetic iron oxide nanoparticles) are themselves good T_2 contrast agents, but coupling them with reduced graphene oxide prevents their clumping thus improving their circulation time and efficiency.[15] As stated earlier about the toxic nature of Gd^{3+} ions, on coupling Gd_2O_3 with GO, the release of Gd^{3+} ions can be eliminated while enhancing the solubility in aqueous solutions.

In continuation of our research work on the diverse applications of nanomaterials in the biomedical arena,[16–26] the recent advances of graphene-based magnetic nanocarriers as potential MRI contrast agents are summarized comprising assorted methods for the preparation of GO as well as graphene-based nanocomposites. The prominent features and magnetism of various graphene-based novel MRI contrast agents are presented in Table 1, along with brief coverage on their theranostic applications and cytotoxicity aspects to assess their biocompatibility.

2. Graphene oxide and graphene-decorated magnetic nanocomposites

2.1 General introduction

Graphene is the most reactive allotrope of carbon and is a two-dimensional entity that is only one atom thick.[27] The carbon atoms are packed in a hexagonal array, forming a honeycomb-like appearance. The hybridization of each carbon atom is sp^2 and each forms three σ-bonds with its adjacent atoms and a π-bond which is directed out of the plane.[13] It exhibits remarkable electrical, optical, and mechanical properties,[28–35] with the notable features being its large specific surface area. Graphene oxide, an oxidized form of graphene, or, a monolayer of graphite, has sp^2-hybridized as well as sp^3-hybridized carbon atoms.[36] The existence of functional groups like hydroxyl, epoxide on the surface, and the carboxylic acid (COOH) group at the edges induce typical hydrophilic behavior. As a result, GO exhibits high dispersibility in aqueous media,[37,38] and can be deployed in biomedical applications as the cavities on the surface make GO an ideal platform to anchor an assortment of nanoparticles. Reduced graphene oxide (rGO), the reduced form of GO, has very few oxygen-containing functional groups. It is hydrophobic and has low dispersibility in aqueous media although it has a high specific surface area, almost like that of pure graphene.[39,40] The nanoparticles can be attached to them by π–π stacking and non-covalent bonding. Graphene-based nanocomposites often have graphene/graphene oxides as substrates with the required nanomaterials incorporated with them. The fabrication and applications of graphene-based nanoparticles

Table 1 Features of various graphene-based novel MRI contrast agents

S. No.	Nanomaterial	Type of magnetism	Highlights/remarks	Ref.
1	Gd_2O_3/GO nanocomposites	Paramagnetic	• Synthesized through a solvent evaporation method • Application as a T_1 contrast agent • Good biocompatibility	6
2	SPION–rGO composite	Superparamagnetic	• A prospective T_2 contrast agent with good stability in human serum • *In vitro* tests with GL261 and J774 cell lines reveal no significant toxicity	15
3	GO–$CoFe_2O_4$	Superparamagnetic	• Biocompatible towards the MCF-7 cell lines	45
4	GO–Fe_3O_4 nanocomposite	Superparamagnetic	• A potential T_2 contrast agent • Biocompatible with normal cells but exhibits toxicity towards breast cancer cells	46
5	GO–PCA/$MnCe_{0.5}Fe_{1.5}O_4$	Superparamagnetic	• Supreme colloidal stability • Notable sensitivity in T_2 and T_2^* MR images • Efficient cellular uptake	47
6	GO-*g*-PCA/γ-Fe_2O_3	Superparamagnetic	• Exhibits excellent stability and extra dispersibility • Finds application as a T_2 MRI contrast agent • No significant cytotoxicity	50
7	uGO@Fe_3O_4	Superparamagnetic	• Exhibits a certain level of toxicity	58
8	$CoFe_2O_4$–rGO nanocomposite	Superparamagnetic to ferromagnetic transition is observed	• A potential T_2 contrast agent in MRI • Doubles the proton relaxivity rate	59
9	Gd_2O_3/GQD nanocomposite	Paramagnetic	• A potential dual-mode contrast agent in MRI • Good biocompatibility and remarkable colloidal stability	60
10	GO–DTPA–Gd	Paramagnetic	• Facilitates simultaneous multimodal T_1-weighted MR/fluorescence imaging and therapeutics • Exhibits significant toxicity towards cancer cells (HepG2) on loading with the anticancer drug, Doxorubicin (DOX)	69
11	GO–DOTA–Gd complexes	Paramagnetic	• Improved T_1 relaxivity • Efficient cellular labeling capacity	70
12	GNP-Dex (Mangradex)	Superparamagnetic	• Exhibits remarkable and sustained contrast enhancement at a high magnetic field with a low paramagnetic ion concentration • No significant allergic response was induced in small animals	71–73
13	Gd^{3+}@CGO	Paramagnetic	• Can produce a bright T_1-weighted image	14
14	Fe_3O_4–GO composite (aminodextran-coated Fe_3O_4 nanoparticles on GO)	Superparamagnetic	• Potential application as an efficient cellular MRI contrast agent with enhanced T_2 relaxivity	42
15	GO-PEG-β-FeOOH nanocomposite	Synergetic magnetism	• Ultra-high transverse relaxivity value (r_2) • Effectively taken up by HeLa cells	74
16	r-GO-ATA-Fe_2O_3 composites	Superparamagnetic	• An effective multifunctional platform for magnetic resonance imaging	75
17	GO/Dual nanocomposite	Superparamagnetic	• Prepared by co-loading GO with Mn-doped Fe_3O_4 and MnO NPs for use as dual T_1–T_2 MRI contrast agents	76
18	IUdR/NGO/SPION/PLGA	Superparamagnetic	• Application as an MRI contrast agent and facilitates glioma-targeted drug delivery	77
19	GO–Fe_3O_4 conjugates	Superparamagnetic	• A multifunctional nanocomposite for drug delivery, cancer sensing, and dual magnetic resonance/fluorescence imaging	78
20	Fe_3O_4/GO nanocomposites	Superparamagnetic	• An effective multifunctional nanoplatform for MRI and pH-responsive drug delivery • High drug loading capacity of 0.37 mg mg^{-1}	41
21	Fe_3O_4/Graphene nanocomposite	Superparamagnetic	• Unique hydrophilic surface structure • A potential T_2 contrast agent • Exhibits excellent biocompatibility	79
22	$MnFe_2O_4$/GO nanocomposite	Superparamagnetic	• A promising T_2 contrast agent, suitable for magnetic hyperthermia	80
23	RGO–IONP–PEG	Superparamagnetic	• Application as an effective theranostics nanoprobe for *in vivo* multimodal imaging-guided photothermal therapy	81
24	RGI-$_{1.8k}$-ICG	Superparamagnetic	• An efficient nanoplatform for drug loading, imaging agent for magnet-responsive cancer treatment	82
25	Functionalized GO/Fe_3O_4 hybrids	Superparamagnetic	• An effective nanoprobe for T_2-weighted cellular MRI and fluorescence labeling	83
26	FGO-Lino-CUR	Paramagnetic	• Application as a nanocarrier for the anticancer drug-linoleic acid–curcumin conjugate and a potential T_2 MRI contrast agent for breast cancer theranostics	84
27	GAGPAu	—	• A potential T_1 contrast agent • Significantly cytotoxic towards HepG2 but nontoxic towards standard fibroblast cell lines (3T3)	85
28	GO-IONP-PEG-DOX (GIPD)	Superparamagnetic	• A theranostic nanoplatform with combined chemo-photothermal anticancer efficacy • Endowed with T_1/T_2 bimodal imaging functions	86
29	GO/Fe_3O_4 nanocomposites	Superparamagnetic	• A prospective magnetic nanocarrier for drug loading and T_2-weighted MRI contrast agent	87
30	5-Fu/SPION/NGO@PCL−LMWC	Superparamagnetic	• Promising nanocarrier for magnetic targeting, drug delivery	88

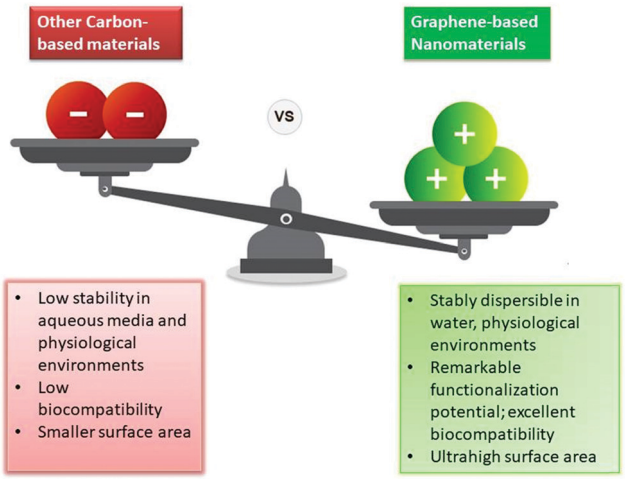

Fig. 2 Comparison of graphene-based nanomaterials with other carbon-based materials.

are promising fields of research. Graphene oxide nanosheets combined with certain nanoparticles were seen to have various advantages such as colloidal stability and desired biocompatibility.[41] Graphene-based materials (GBMs), due to their remarkable properties,[42] have many advantages over other systems (Fig. 2).

2.2 Strategies for the synthesis of graphene oxide and graphene-decorated magnetic nanocomposites

The strategies for the synthesis of graphene oxide and graphene-decorated magnetic nanocomposites are discussed here in brief.

2.2.1 Methods of synthesis of graphene oxide (GO)

Hummers' method. Hummers' method is a common method for the preparation of graphite oxide, where $KMnO_4$ solution is added to a mixture of graphite, $NaNO_3$, and H_2SO_4 as depicted in Fig. 3.[43,44] Venkatesha *et al.* synthesized GO–$CoFe_2O_4$ in a two-step protocol wherein Hummers' method was employed for the synthesis of GO. It was then intercalated with $CoFe_2O_4$ to form ultrafine GO–$CoFe_2O_4$ nanocomposites which were used as T_1 and T_2 MRI contrast agents.[45] In another study, the same group prepared GO–Fe_3O_4 nanoparticles with a high transverse proton relaxivity value.[46]

Modified Hummers' method. Torkashvand *et al.* synthesized GO using a modified version of Hummers' method. They prepared polymerized $MnCe_{0.5}Fe_{1.5}$ nanoferrofluid loaded on graphene oxide which was used as T_2 and T_2^* weighted MRI contrast agents.[47] Llenas *et al.* synthesized GO using a modified version of Hummers' method. The GO was decorated onto the SPION to produce the SPION–GO hybrid which is a good T_2 contrast agent.[15]

Mildly method. Mildly method, an improved Hummers' method, deploys a lesser concentration of the oxidizing agent,[48,49] as illustrated by Torkashvand *et al.* in the preparation of graphene oxide-grafted poly citric acid-γ-Fe_2O_3 {GO-*g*-PCA/γ-Fe_2O_3} nanoparticles as an MRI contrast agent.[50]

2.2.2 Methods for the synthesis of graphene-decorated magnetic nanocomposites

Hydrothermal method. The hydrothermal method is a very common method for the synthesis of all types of assorted

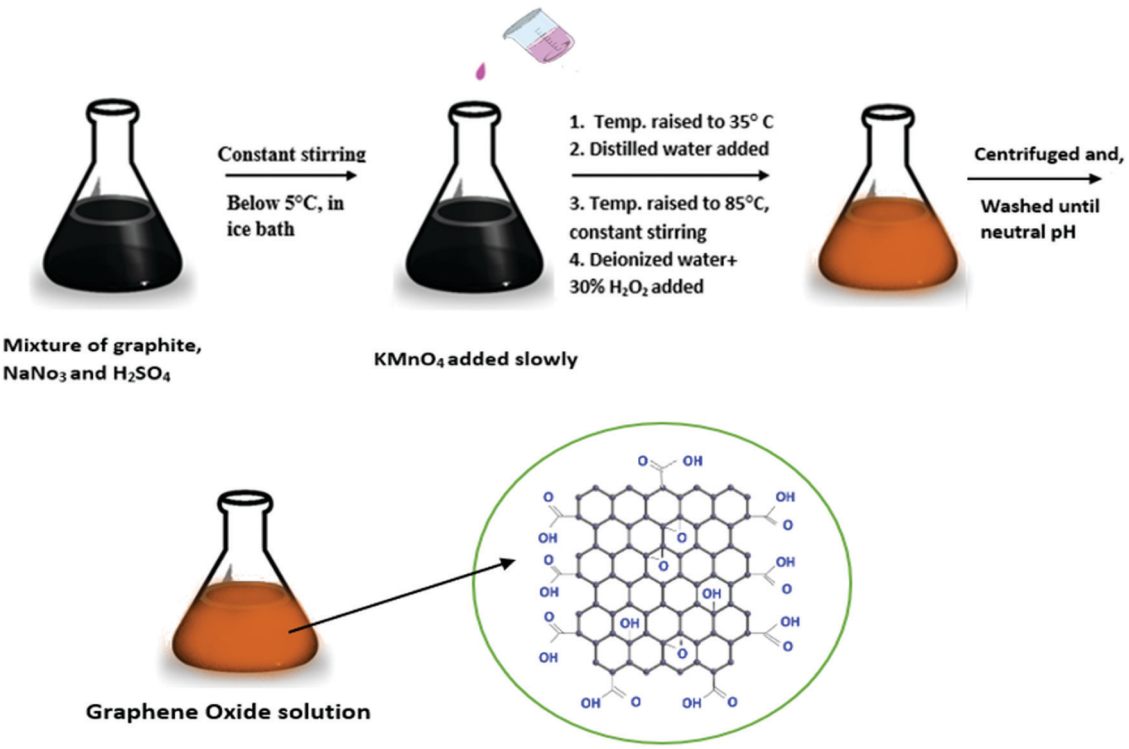

Fig. 3 Hummers' method for the preparation of graphene oxide (GO).

nanoparticles,[51–55] and is superior to others as it can generate stable nanocomposites at high temperatures.[56] The added advantage is that the applied elevated temperature and pressure not only induce the formation of nanocrystals but also simultaneously reduce GO to rGO to some extent.[57] Shen *et al.* synthesized uGO@Fe_3O_4 (ultrafine graphene oxide–iron oxide) nanoparticles in which the GO nanoparticles were synthesized by a hydrothermal method. uGO@Fe_3O_4 is used as an MRI contrast agent as well as a drug delivery vehicle.[58] Alazmi *et al.* prepared $CoFe_2O_4$–rGO nanoparticles, for use as T_2 contrast agents in MRI, through a hydrothermal method using water as the solvent and by adding stoichiometric amounts of $Co(NO_3)_2{\cdot}6H_2O$ and $Fe(NO_3)_3{\cdot}9H_2O$ to the GO aqueous dispersion.[59]

Thermal cutting method. Wang *et al.* employed the thermal cutting method for the synthesis of two-proton graphene quantum dots (GQDs). The GO solution was diluted and ultrasonicated to homogenize the solution and to lower the average size of the GO nanoparticles. Then the GO powder was obtained from the solution by freeze-drying. The GO powder in DMF was ultrasonicated to homogenize and was placed in an autoclave and heated to 200 °C. Upon cooling to room temperature, it was centrifuged and washed with deionized water. The GQD modified Gd_2O_3 prepared by them has been used as a dual-mode MRI contrast agent and a cell labeling agent.[60]

The relative advantages and shortcomings of various methods for the preparation of graphene oxide and graphene-based magnetic nanocomposites are listed in Fig. 4.

3. T_1 and T_2 contrast agents

Contrast agents help in improving the sensitivity, accuracy, and specificity of magnetic resonance imaging (MRI), by altering the time of relaxation of water protons.[61] T_1 or positive contrast agents reduce the relaxation time of the longitudinal component of magnetization (longitudinal or spin–lattice relaxation time), thereby producing enhanced signal intensity on T_1-weighted images.[62] Paramagnetic contrast agents based on Gd(III), Mn(II), and metal-chelates are most often used as T_1 contrast agents. These contrast agents function as hepatobiliary agents, agents in the blood pool as well as extracellular fluids.[63] T_2 or negative contrast agents shorten the relaxation time of the transverse component of magnetization (transverse or spin–spin relaxation time) which causes a decreased signal intensity on T_2-weighted images.[5,62] Superparamagnetic iron oxide nanoparticles (SPIONs) are nanoparticles of magnetite (Fe_3O_4) or maghemite (γ-Fe_2O_3), with their size in the range of 50–180 nm, and are among the most commonly employed T_2-weighted contrast agents besides ferrites. Ultrasmall SPIONS with a core size less than 50 nm can be effectively employed as T_1 contrast agents.[64–67] The comparison between T_1- and T_2-weighted magnetic resonance (MR) imaging is presented in Fig. 5.

The effectiveness of these contrast agents depends on the relaxivity which indicates the change in relaxation time as a function of contrast agent concentration. r_1 relaxivity corresponds to changes in longitudinal relaxation time and r_2 corresponds to changes in transverse relaxation time upon the addition of T_1 and T_2 contrast agents, respectively. The

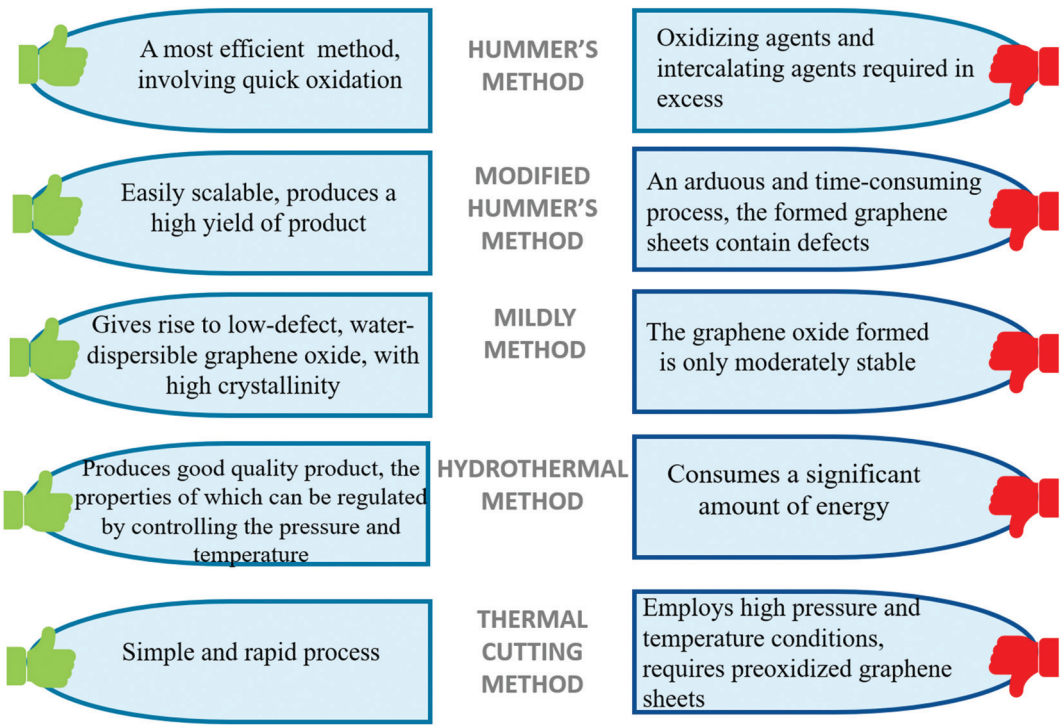

Fig. 4 Advantages and disadvantages of various methods for the preparation of graphene oxide and graphene-based magnetic nanocomposites.

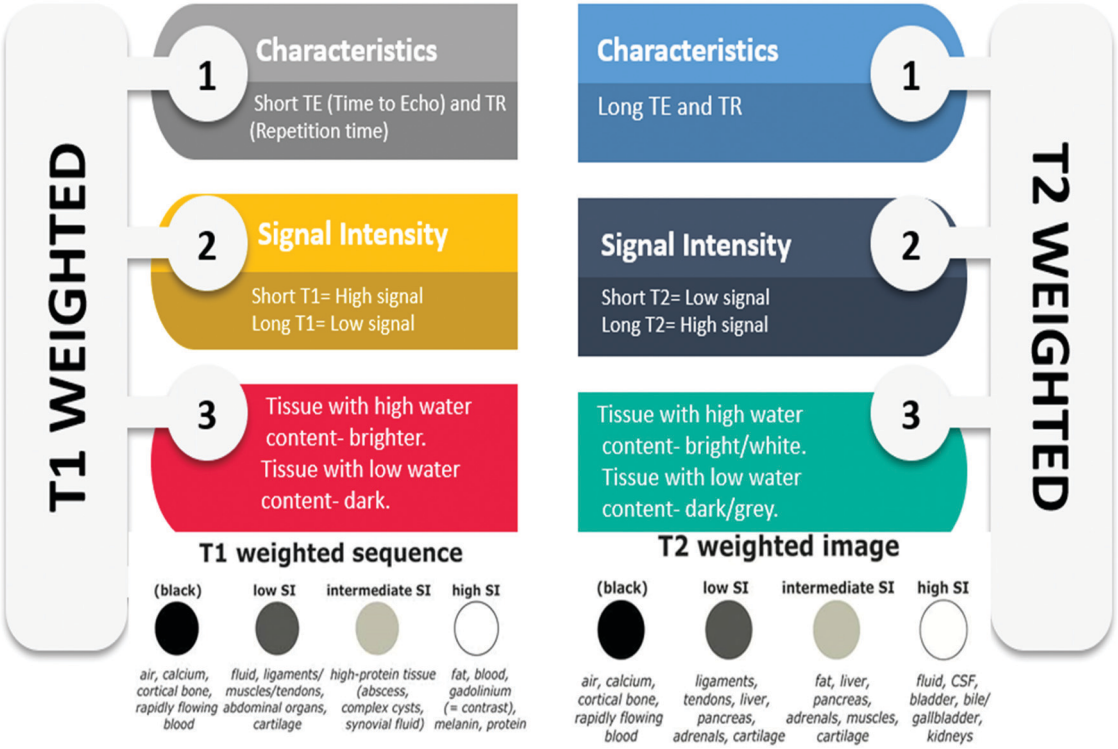

Fig. 5 Comparison between T_1 weighted and T_2 weighted MR imaging.

relaxivity ratio, r_2/r_1, determines the type of the contrast agent, whether positive (T_1) or negative (T_2). The contrast agents which have $r_2/r_1 < 5$ are categorized as T_1 contrast agents, whereas those which have a high r_2/r_1 ratio (>10) are categorized as T_2 contrast agents.[68]

3.1 T_1 contrast agents adorned on graphene

T_1 or positive contrast agents shorten the longitudinal relaxation time (or spin–lattice relaxation time) of the nearby water protons in the areas of tissue where accumulation occurs, thus providing brighter images.[89] The longitudinal relaxation denotes the realignment of the longitudinal component of magnetization with the applied magnetic field. The majority of the clinically used MRI contrast agents are paramagnetic metal chelates comprised of gadolinium (Gd). Magnevist (Gd-DTPA) is an FDA-approved contrast agent and is the most commonly employed T_1 clinical contrast agent. But these contrast agents have a short circulation time, low cellular labeling capacity, and possess potential toxicity *in vivo*, which may affect the cardiovascular system, cause cerebral deposition, or may cause nephrogenic systemic fibrosis.[90–96] As an alternative to Gd, complexes of manganese (Mn^{2+}) are employed, which are relatively less toxic. Gd^{3+} contains 7 unpaired electrons in the valence f-orbitals and has a high spin quantum number of 7/2. In contrast, Mn^{2+} has 5 unpaired electrons in the 3d subshell and possesses a notable spin quantum number (S = 5/2). Both of them have large magnetic moments, high longitudinal relaxation time ($\sim 10^{-8}$ s), quick water kinetics, and fail to exhibit magnetization exchange when no external magnetic field is present. Fe^{3+}, with 5 unpaired electrons in the d-subshell, also displays these characteristics and is at times used to make T_1 contrast agents.[62,93,97,98]

Various experiments have revealed that anchoring these paramagnetic nanoparticles on GO helps in reducing the toxicity of contrast agents comprising heavy metal ions, which can be attributed to the reduced release rate.[99] Wang *et al.* prepared gadolinium oxide (GDO)/GO nanocomposites, using spherical and plate-like GDO nanoparticles on GO sheets, of core sizes 3 nm and 17 nm, respectively. The relaxivity values measured using a 7T MRI scanner were 34.48 mM^{-1} s^{-1} and 21.60 mM^{-1} s^{-1}, respectively. The water-soluble GDO/GC nanocomposites were formed by π–π stacking between the hydrophobic Gd_2O_3 NPs and hydrophobic basal planes of GO. By precisely adjusting the mass ratio of nanoparticles to GO, the amount of nanoparticle loading on the graphene oxide sheets could be regulated. The cytotoxicity test revealed that these nanocomposites have better biocompatibility than the commercially used and other known Gd-based contrast agents.[6]

The results also show that such graphene-based contrast agents show substantially higher relaxivity, r_1 values than the clinically used T_1 contrast agents (Table 2).[12,62] Since graphene has a high density of oxygen-containing functional groups as well as cavities, the metal ions can be easily chelated with it or can be buried between the layers.[95]

One of the initially reported graphene-based T_1 contrast agents was synthesized by Zhang *et al.* *via* conjugation of diethylenetriaminepentaacetic acid (DTPA) with GO, and subsequent complexation of Gd(III). This nanosized GO–DTPA–Gd

Table 2 Various graphene-based magnetic nanocomposites as T_1 contrast agents in MRI

S. No.	Nanomaterial	Size (nm)	Magnetic field (T)	Relaxivity, r_1 (mM^{-1} s^{-1})	Ref.
1	GO–DTPA–Gd Complex	1	11.7	10.8	69
2	GNP-Dex (Mangradex)	3	7	92	71–73 and 100
3	GDO–GO	3	7	34.48	6
		17	7	21.60	
4	GO–DOTA–Gd Complex	20–50	11.7	14.2	70
5	Gd^{3+}@CGO	7–15	3	63.8	14

complex could be internalized into cells, enabling cellular magnetic resonance imaging, and it showed an r_1 value of 10.8 mM^{-1} s^{-1} at 11.7 T. A few years later, the same group prepared a better GO–DOTA–Gd complex for use as a T_1 contrast agent, mainly aimed at stem cell labeling. DOTA (1,4,7,10-tetraazacyclododecane-1,4,7,10-tetraacetic acid) being a macrocyclic ligand as opposed to a linear DTPA molecule, has better kinetic stability and facilitates Gd(III) complexing and exhibiting a relaxivity r_1 value of 14.2 mM^{-1} s^{-1} at 11.7 T. The increased relaxivity may be attributed to the use of ultrasmall GO sheets which provide a higher edge-to-area ratio for chelation of Gd to the active reaction sites.[69,70]

Kanakia *et al.* prepared water-dispersible Mn^{2+} intercalated graphene nanoparticles functionalized with dextran *via* non-covalent interactions (GNP-Dex or Mangradex). The r_2/r_1 ratio was 2.2 and it exhibited a high r_1 relaxivity value of 92 mM^{-1} s^{-1} (at 7 T) with GNP-Dex being stable in blood and biological fluids. They analyzed the *in vitro* physicochemical characteristics. As a follow-up, dose-range findings and safety pharmacology assessments were performed by intravenously administering it in rats (Fig. 6). In 2015, the sub-acute toxicity

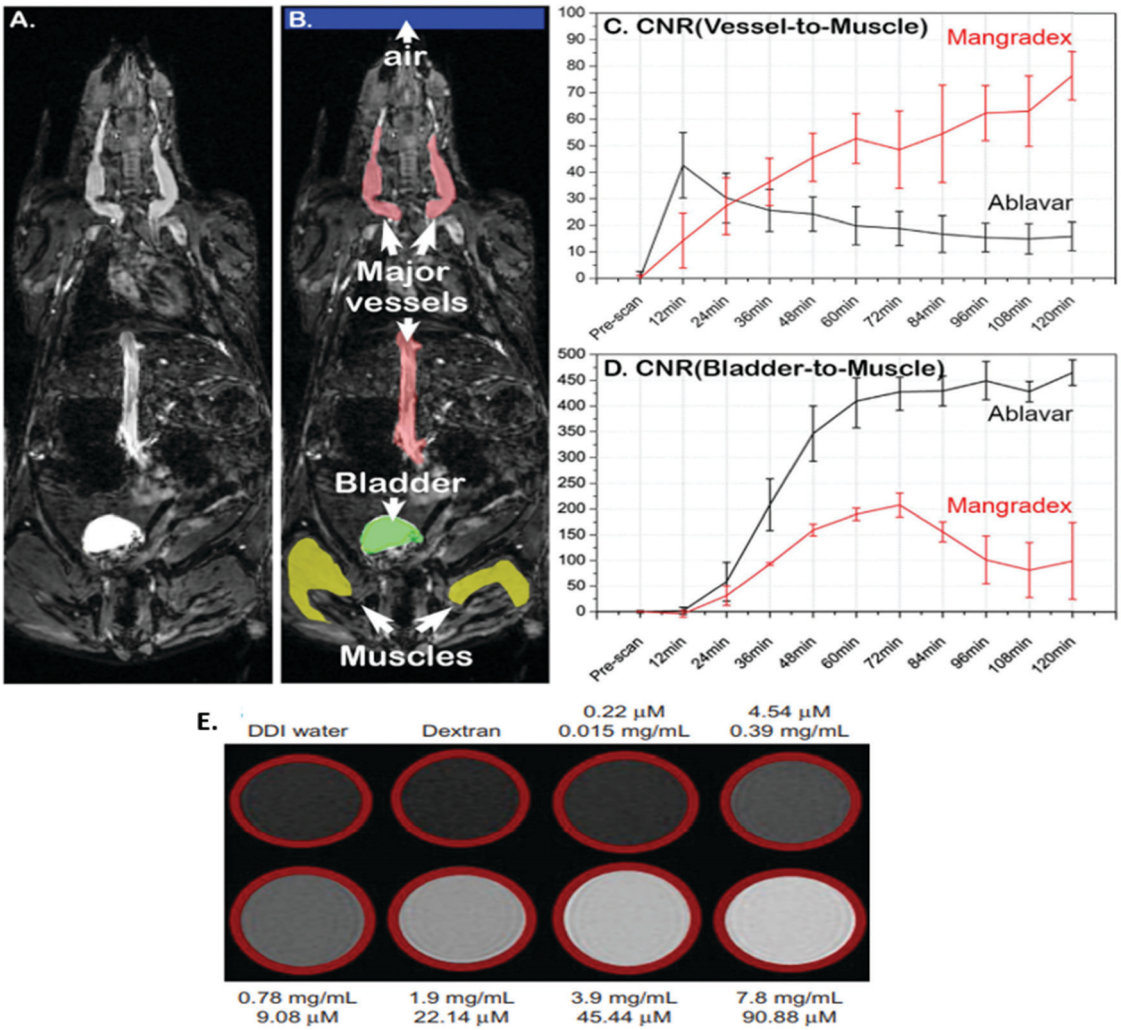

Fig. 6 (A) MRI image of a horizontal section covering the whole mouse body. (B) Regions of Interest (ROI) of the most important parts of the mouse body relevant to the study. (C) A plot showing the contrast preeminence and the sustained effect of Mangradex assessed in large vessels compared to the clinical blood pool agent Ablavar during serial imaging analysis. (D) A time curve to compare the apparent excretion of both the contrast agents expected through the bladder. (E) T_1-weighted MR phantom images of Mangradex. The top (A–D) figures are reprinted from ref. 73 and the bottom € figure is reprinted with permission from ref. 100 Copyright 2015 Nature Publishing Group and Copyright 2013 Dove Press, respectively.

and contrast enhancement ability were assessed in small animals, and the positive results obtained rendered Mangradex a prospective MRI contrast agent.[71–73,100]

The presence of oxygen-containing functional groups bestows GO with significant dispersibility in aqueous media. Through conversion of the hydroxyl and epoxy groups of graphene oxide to carboxyl groups, carboxyl-functionalized graphene oxide (CGO) can be prepared which advantageously exhibits enhanced water dispersibility. Ren *et al.* synthesized a novel MRI contrast agent making use of CGO as a nanocarrier to directly interact with $GdCl_3.6H_2O$; the resulting Gd^{3+}@CGO possessed a relaxivity value of 63.8 mM^{-1} s^{-1} (at 3 T), which is more than that of Magnevist by a factor of 14 (relaxivity value of Magnevist = 4.5 mM^{-1} s^{-1}). Furthermore, Gd^{3+} anchored on CGO can maintain stability for at least a year.[14]

3.2 T_2 contrast agents adorned on graphene

T_2 or negative contrast agents accelerate the spin–spin relaxation of water protons, and hence reduce their transverse relaxation time. In the past decade, iron-based MNPs have been used as contrast agents for T_2-weighed MR imaging.[74] Superparamagnetic Fe_3O_4 nanoparticles function as an outstanding MRI contrast agent and are frequently employed in the biomedical field.[1,101] However, when used *in vivo*, Fe_3O_4 NPs tend to aggregate and precipitate inside the body vessels resulting in reduced circulation time in blood.[42,102] To overcome this issue, Chen *et al.* employed a GO-based platform to anchor aminodextran (AMD) coated Fe_3O_4 NPs and found that aggregation of Fe_3O_4 NPs on GO sheets enhanced the physiological stability as well as T_2 relaxivity of the nanoparticles to a great extent.[1] To increase their T_2 relaxivity, Venkatesha *et al.* synthesized three different reaction mixtures containing 0.01 g, 0.1 g, and 0.2 g of GO, and the highest proton relaxivity, r_2 = 267.1 mM^{-1} s^{-1}, was obtained for the mixture containing 0.1 g of GO. This was due to the large number of carboxyl groups and the large number of NPs within GO.[42,46]

In situ growth of β-FeOOH nanorods on GO increased the relaxivity value of β-FeOOH nanorods by about 60 times, as demonstrated by Chen *et al.,* wherein GO-PEG-β-FeOOH was found to exhibit an ultra-high transverse relaxivity value of 303.81 mM^{-1} s^{-1}.[74] This nanocomposite can serve as an excellent contrast agent for non-invasive *in vivo* MRI. Wang *et al.* produced GO–$CoFe_2O_4$ nanocomposites (Fig. 7) by precipitating $CoFe_2O_4$ NPs with a diameter of 5–13 nm in the presence of GO which showed a significant T_2 relaxivity value of 92.7 mM^{-1} s^{-1}. The value of relaxivity first increased and then decreased with reflux time.[103] These nanocomposites were found to be biocompatible towards the MCF-7 cell line.

GO exhibits a fairly biocompatible surface and serves as a promising platform to anchor magnetic NPs but reduced graphene oxide (rGO) is relatively chemically inert. Alazmi and co-workers initially assessed the proton relaxivity value obtained in $CoFe_2O_4$–rGO nanocomposites.[59] They studied the effect on proton relaxivity by using two different types of rGO; rIGO and rHGO at various concentrations of $CoFe_2O_4$ (Table 3). The highest value of proton relaxivity, r_2 = 102.1 mM^{-1} s^{-1} was shown by a sample of 30 wt% $CoFe_2O_4$–rIGO (Fig. 8).

Torkashvand *et al.* synthesized GO and polymerized it with citric acid (GO-*g*-PCA) and used it as a substrate for the loading of NPs.[47,50] GO-*g*-PCA/γ-Fe_2O_3 nanocomposite was synthesized which was found to exhibit higher stability and excellent dispersibility with r_2 and r_2^* values of 125.63 and 280.85 mM^{-1} s^{-1},

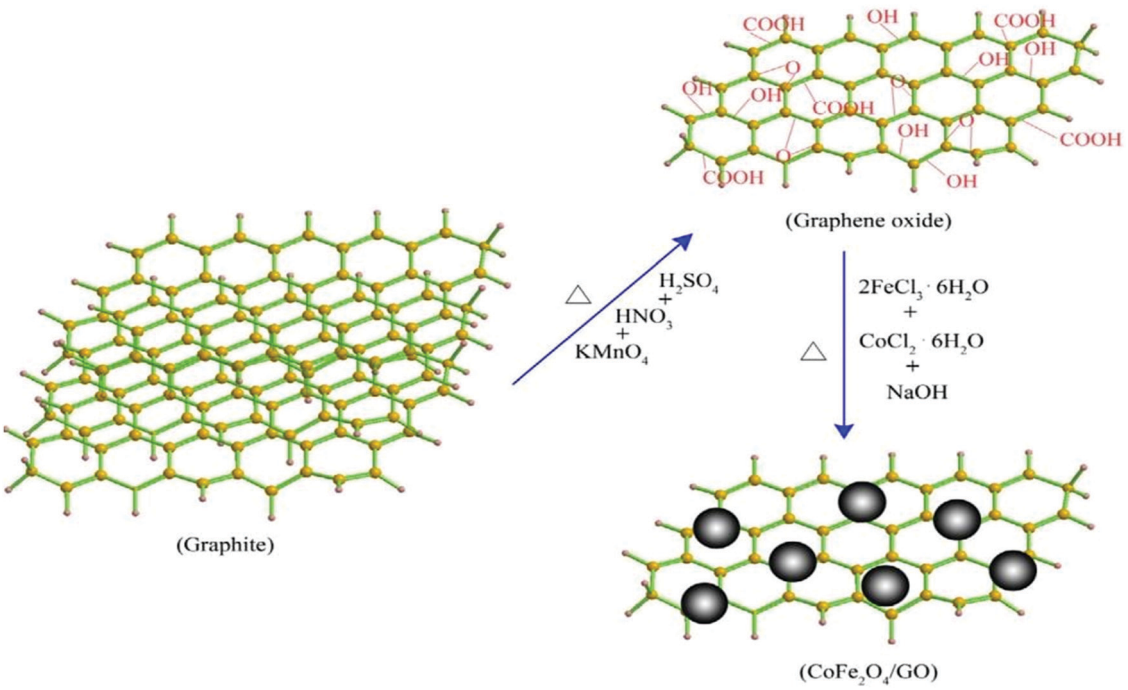

Fig. 7 Schematic representation for the synthesis of $CoFe_2O_4$/GO. Reprinted with permission from ref. 103 Copyright 2015 Elsevier.

Table 3 Various graphene-based magnetic nanocomposites as T_2 contrast agents in MRI

S. No.	Nanomaterial	Size (nm)	Magnetic field (T)	Relaxivity value, r_2 (mM^{-1} s^{-1})	Ref.
1.	GO-*g*-PCA/γ-Fe_2O_3	20	3.0	125.63	50
2.	GO–PCA/$MnCe_{0.5}Fe_{1.5}O_4$	32	3.0	109.15	47
3.	$CoFe_2O_4$/graphene oxide	13	3.0	92.7	103
4.	Fe_3O_4–GO composite	174	11.7	76	101
5.	GO-PEG-β-FeOOH	3	7.0	303.81	74
6.	$CoFe_2O_4$–rHGO				59
	5wt% metal oxide	3.1	11.7	8.8	
	10wt% metal oxide	3.4		16.7	
	16wt% metal oxide	4.3		33.7	
	30wt% metal oxide	6.8		55.6	
7.	$CoFe_2O_4$–rIGO				59
	5wt% metal oxide	5.3	11.7	17.4	
	10wt% metal oxide	7.4		21.4	
	16wt% metal oxide	9.2		43.6	
	30wt% metal oxide	12.4		102.1	
8.	GO–Fe_3O_4 composite				46
	0.01g GO	11.4	1.5	45.7	
	0.1g GO	9.3		267.1	
	0.2g GO	8.5		92.3	
9.	Fe_3O_4/G nanocomposite	—	3	123.04	79

respectively, at 3.0 T.[50] Another nanoferrofluid GO–PCA/$MnCe_{0.5}Fe_{1.5}O_4$ was prepared by loading $MnCe_{0.5}Fe_{1.5}O_4$ NPs on the surface of GO–PCA that displayed extra colloidal stability and high dispersibility with a high saturation magnetization (M_s) of 47.8 emu g^{-1}.[47] The r_2 and r_2^* values were found to be 109.15 and 180.23 mM^{-1} s^{-1}, respectively. Idisi *et al.* synthesized r-GO-ATA-Fe_2O_3 composites and studied their various properties[75] including superparamagnetic behavior, because of which these nanocomposites can serve as potential contrast agents for MRI.

In 2016, Zan *et al.* reported for the first time a one-pot synthesis of water-soluble and non-toxic Fe_3O_4/G nanocomposites with a high T_2 relaxivity value of 123.04 mM^{-1} s^{-1} as a promising MRI contrast agent; the nanocomposites exhibited appreciable stability and biocompatibility.[79]

Peng and co-workers prepared water-soluble $MnFe_2O_4$ nanoparticles (MFNPs)/GO nanocomposites (denoted as MGONCs) by anchoring hydrophobic MFNPs on GO sheets. It was demonstrated that the loading of MFNPs and the hydrodynamic size of the nanocomposites can be adjusted by varying the ratio of magnetic NPs to GO and the sonication time, respectively. The MGONCs were loaded with MFNPs of 6 nm, 11 nm, and 14 nm. The highest T_2 relaxivity value of r_2 = 256.2 mM^{-1} s^{-1} was obtained with an MFNP of 14 nm at a 0.25 mM iron concentration. After PEGylation, the nanocomposite was found to exhibit excellent colloidal stability in physiological solutions.[80]

3.3 Dual-mode MRI contrast agents adorned on graphene

Dual MRI contrast agents are used to markedly enhance the MRI contrast efficiency. They also help mitigate the drawbacks of single T_1 and T_2 contrast agents. Though T_1-weighted images exhibit remarkable positive contrast and provide high spatial resolution, the potential toxicity due to the release of free metal ions like Gd^{3+} and short blood circulation times are some of the undesirable traits.[45,64,104,105] T_2-Weighted images show better detection of lesions but, the high magnetic moment of the nanoparticles of T_2 contrast agents causes a blurring effect and may adversely affect the interpretation of the magnetic resonance image obtained.[35,76,106] So, dual T_1–T_2 contrast agents are used for more accuracy and enhanced biocompatibility (Table 4). Peng *et al.* demonstrated the synthesis of a novel dual T_1–T_2 contrast agent by simultaneously decorating Mn-doped Fe_3O_4 and MnO magnetic nanoparticles onto graphene oxide sheets (Fig. 9). The r_1 and r_2 relaxivity values obtained using a 7 T MRI scanner were 5.16 mM^{-1} s^{-1} and 300.62 mM^{-1} s^{-1}, respectively.[76] Venkatesha *et al.* illustrated that $CoFe_2O_4$ decorated on graphene oxide for use as T_1 and T_2 contrast agents is biocompatible towards the MCF-7 cell line.[36] Wang *et al.* reported the synthesis of dual-mode Gd_2O_3/GQD nanocomposites (Fig. 10) which showed remarkable water solubility and biocompatibility.[60]

4. Multifunctional MRI contrast agents adorned on graphene

In recent years, there has been growing interest in the development of versatile theranostic nanoplatforms, which help in diagnosis and therapy.[107] The high specific surface area and remarkable functionality features of GO allow an ultrahigh loading capacity of drugs on its surface.[108] Zhang *et al.* reported the synthesis of a GO–DTPA–Gd complex which is capable of cellular MR imaging, with improved T_1 relaxivity and it exhibited a high drug loading capacity (70%) for the anticancer drug, doxorubicin (DOX). The GO–DTPA–Gd/DOX displayed significant toxicity to cancer cells (HepG2) (Fig. 11).[69] The prospective T_2 contrast agent, the GO–$CoFe_2O_4$ nanocomposite, prepared by Wang *et al.* also functions as a multifunctional probe for cancer theranostics.[103] On loading DOX, the nanocarrier showed a high drug loading capacity of 1.08 mg mg^{-1} and hence it can be regarded as a promising candidate for drug delivery as well. Shirvalilou and co-workers prepared a potential MRI contrast agent, IUdR-loaded magnetic NGO/PLGA, capable of effective magnetic targeting of gliomas and therapeutic drug delivery. They assessed the safety and tumor inhibitory efficiency of IUdR by using the C6 glioma cell line and systemic administration in glioblastoma-bearing rats.[77] Gonzalez-Rodriquez *et al.* synthesized GO–Fe_3O_4 nanocomposites that have potential as a T_2 MRI contrast agent, for optical cancer detection, with the capability of excellent pH-sensitive drug delivery. The non-covalently conjugated doxorubicin showed 2.5 times enhanced efficacy.[78]

Wang *et al.* prepared a magnetic Fe_3O_4/GO nanocomposite as an efficacious multifunctional nanoplatform with an excellent MRI enhancement effect and pH-responsive controlled drug delivery. An anticancer drug, 5-Fluorouracil (5-FU) was loaded onto the surface of the nanocarrier and the drug loading capacity was found to be as high as 0.37 mg mg^{-1}.[41] In a later experiment, they developed a targeting peptide-modified

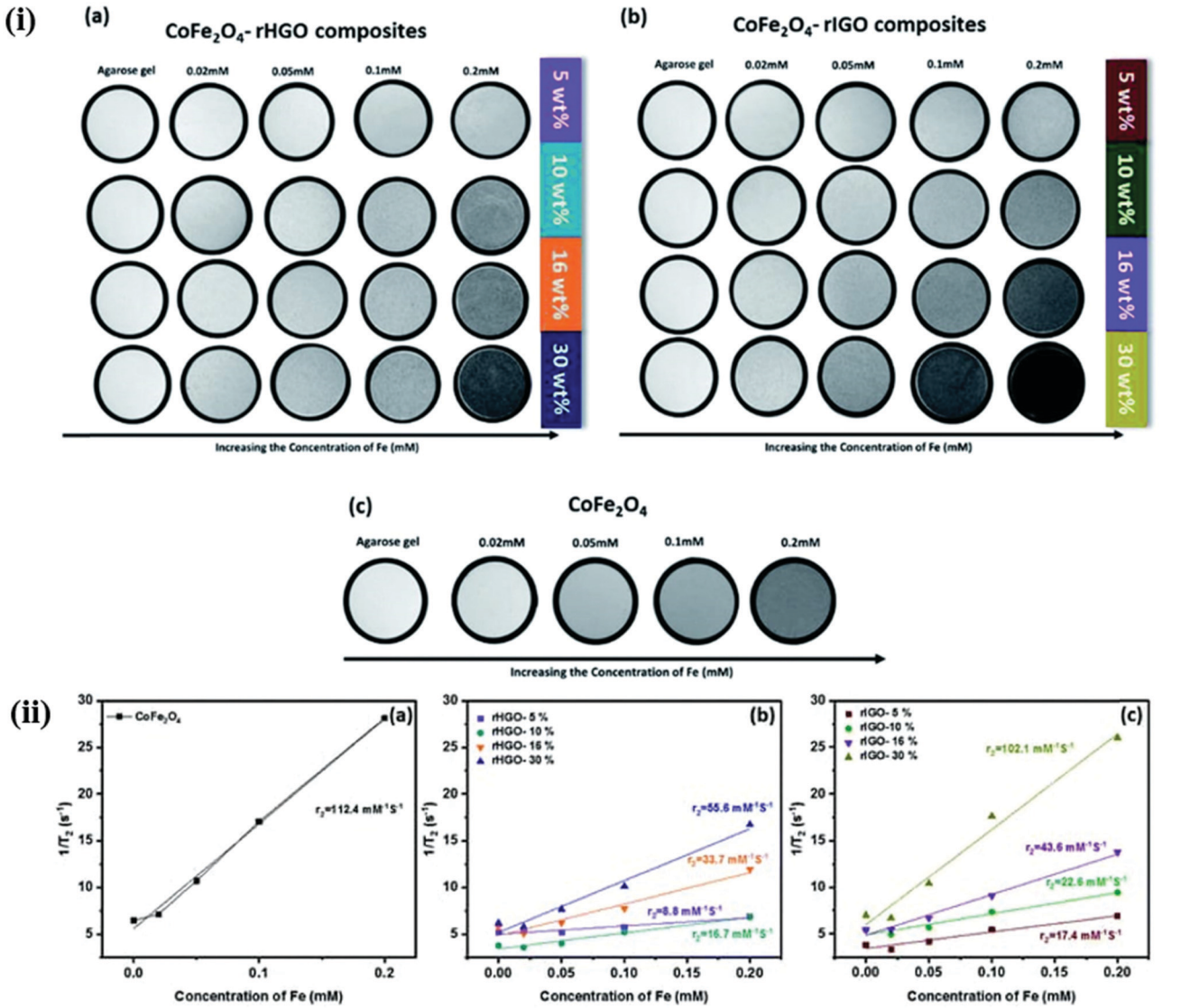

Fig. 8 (i) T_2-Weighted MR images at different Fe concentrations for (a) $CoFe_2O_4$–rHGO composites, (b) $CoFe_2O_4$–rIGO composites and (c) pure $CoFe_2O_4$. (ii) Plot of T_2 relaxation rate r_2 ($1/T_2$) for (a) $CoFe_2O_4$–rHGO composites, (b) $CoFe_2O_4$–rIGO composites and (c) pure $CoFe_2O_4$, suspended in aqueous solution at different Fe concentrations. Reprinted from ref. 59 Copyright 2019 Royal Society of Chemistry.

Table 4 Various graphene-based magnetic nanocomposites as dual T_1–T_2 contrast agents in MRI

S. No.	Nanomaterial	Magnetic field (T)	Relaxivity, r_1 (mM^{-1} s^{-1})	Relaxivity, r_2 (mM^{-1} s^{-1})	Ref.
1	GO/Dual nanocomposite (GO co-loaded with Mn-doped Fe_3O_4 and MnO NPs)	7	5.16	300.62	76
2	Gd_2O_3/GQD nanocomposite	7	15.995	131.02	60
3	GO–$CoFe_2O_4$	1.5	4.73	188.2	45

mesoporous silica with magnetic graphene. The notable properties like high r_2 relaxivity value, facile magnetic separation, high DOX loading capacity, thermo-, and pH-responsive sustained release, make it a robust platform for glioma theranostics.[109]

In another study, Zhou *et al.* prepared water-dispersible GO/Fe_3O_4 hybrids which were further functionalized *via* layer-by-layer assembly.[83] They loaded the surface of the functionalized GO/Fe_3O_4 hybrids with fluorescein isothiocyanate (FITC), a probe for fluorescence labeling, for tracing the cellular internalization of the functionalized GO/Fe_3O_4 hybrids. These hybrids possessed an excellent MRI negative contrast enhancement with an r_2 value of 493 mM^{-1} s^{-1}, besides low cytotoxicity and appropriate biocompatibility.

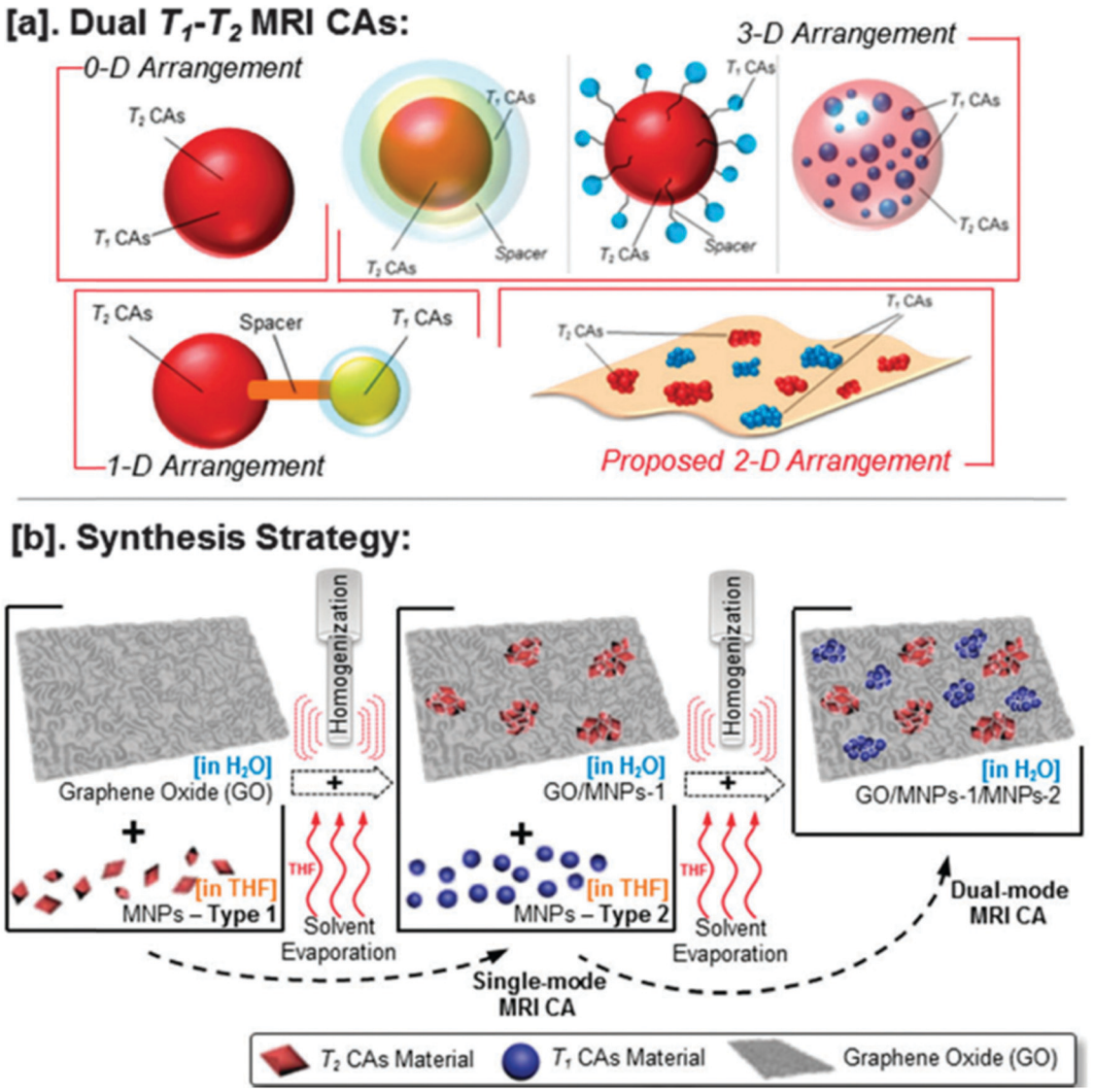

Fig. 9 (a) Illustrations of various T_1–T_2 MRI contrast agent (DMCA) designs. (b) Proposed strategy to fabricate DMCA based on the assembly of T_1 and T_2 nanoparticulate Cas on the two-dimensional GO surface. Reprinted from ref. 76 Copyright 2015 Royal Society of Chemistry.

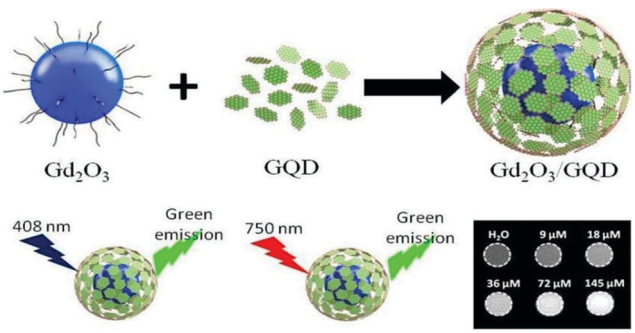

Fig. 10 Dual-mode Gd_2O_3/GQD nanocomposites for use in MRI imaging. Reprinted from ref. 60 Copyright 2018 Royal Society of Chemistry.

In a recent study, Razaghi *et al.* adopted an eco-friendly strategy to prepare fluorinated graphene oxide (FGO) for application in breast cancer theranostics.[84] A remarkable loading capacity of 61.5% rendered FGO as a suitable nanocarrier for loading the synthesized anticancer drug, Linoleic acid–curcumin conjugate (Lino-CUR). The MTT analysis revealed that Lino-CUR exhibited higher cytotoxicity against MCF-7 cells as compared to CUR. The *in vitro* MRI studies revealed that FGO-Lino-CUR can also function as a potential T_2 contrast agent with a significant relaxivity of 67.12 mM^{-1} s^{-1}. *In vivo* anti-tumor efficacy studies carried out on the $4T_1$ induced BALB/c breast cancer model demonstrated that the synthesized theranostic nanoplatform showed better and improved capability for tumor suppression in comparison to free Lino-CUR. Moreover, no notable variation in the body weight of the mice testifies to the safety of the theranostic agent. Sadighian *et al.* prepared GO/Fe_3O_4 nanocomposites with prospective MRI T_2 contrast agent application coupled with pH-dependent controlled release of curcumin.[87] In addition to the antioxidant activity, the high surface area of the nanocomposite offered

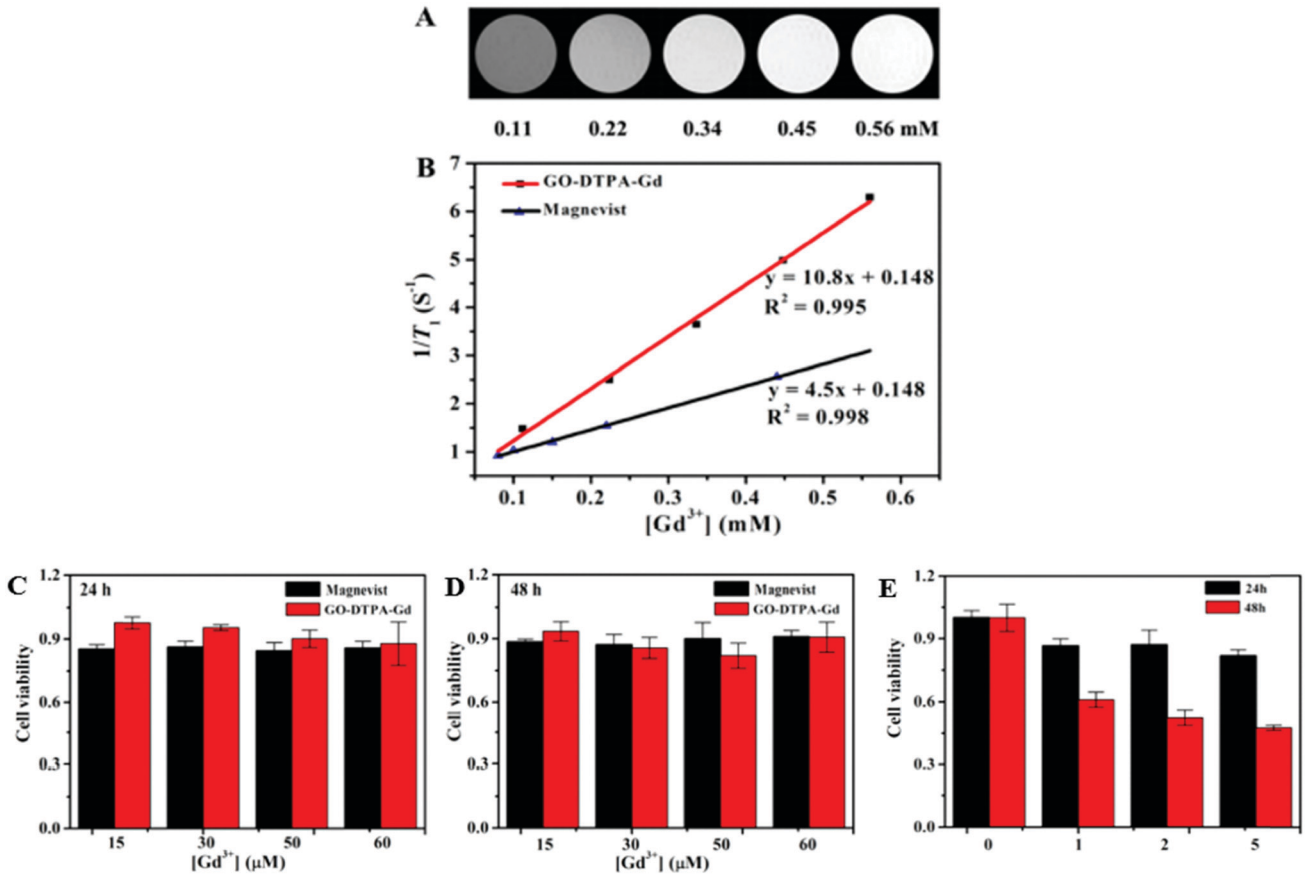

Fig. 11 (A) T_1-Weighted MR images of GO–DTPA–Gd at different Gd concentrations in water. (B) Plot of relaxation rate r_1 *versus* Gd^{3+} concentration for GO–DTPA–Gd and Magnevist. Relative viability of HepG2 cells incubated with GO–DTPA–Gd and Magnevist at different Gd^{3+} concentrations for (C) 24 h and (D) 48 h. (E) Relative viability of HepG2 cells treated with GO–DTPA–Gd/DOX at different DOX concentrations for 24 h and 48 h, respectively. Reprinted with permission from ref. 69 Copyright 2013 American Chemical Society.

efficient loading of the drug (22%) and excellent encapsulation efficiency (96%). MTT analysis showed that the composite manifests significant toxicity and exhibits anticancer properties on Caco-2 cells. Consequently, the cell viability was reduced to less than 50% at a concentration of 140 μg ml^{-1}.

In the last few years, GO-IONP composites have attracted immense interest for their application as a potential contrast agent for MRI of cells and tissues, and also as a nanoshuttle for therapeutic drug delivery.[110] In a recent study, Li *et al.* developed a multifunctional platform based on a magnetic GO nanohybrid for MRI-guided cancer theranostics.[86] According to previous research, only ultrasmall superparamagnetic IONPs with a diameter of less than 5 nm could serve as good T_1 contrast agents.[15] But in this study, IONPs with a diameter of ~8 nm have been precipitated over GO nanosheets. Still, the obtained nanohybrid presented good applicability as both T_1 and T_2 contrast agents. This could be attributed to the greater accessibility of the water molecules to the PO-PEG-decorated IONPs.

Gold nanoparticles (AuNPs) are known for their exceptional attributes such as their high surface area to volume ratio. Alhough AuNPs have been generally employed for CT contrast improvement, Usman *et al.* used them as supporting MRI contrast agents in their work.[88] They developed a GO-based theranostic nano delivery system for MRI, employing gadolinium(III) nitrate hexahydrate (Gd) as the starting material for the contrast agent, and naturally occurring protocatechuic acid (PA) as an anticancer agent. The GAGPA nanocomposite was obtained after the conjugation of Gd and PA, which was further modified to GAGPAu, after coating with Au NPs. In comparison with the pure Gd and water reference, the GAGPAu nanocomposite was found to possess a higher T_1 contrast. It presented great potential as a platform for cancer chemotherapy and diagnosis.

5. Theranostic applications of graphene-based magnetic nanomaterials

Graphene derivatives like GO and rGO display tunable surface chemistry facilitating the incorporation of various magnetic nanoparticles with widespread appliances in the domains of biomedicine, magnetic resonance imaging, fluorescence labeling, hyperthermia, and photothermal therapy.[111] The development of a theranostic nanoplatform that integrates diagnostic

and therapeutic techniques is gaining prominence and is an appealing strategy to accomplish simultaneous diagnosis and treatment.[112] In this context, several graphene-based nanomaterials capable of MRI-guided drug delivery/therapy, and multi-model imaging-guided therapy have been reported in the last few years (Table 5). Multi-model imaging-guided therapy offsets the inherent individual limitations of different diagnostic techniques while combining their virtues, fostering significantly enhanced imaging quality for precise diagnosis and treatment. In this section, we briefly describe some of the theranostic applications of GBMs, with special emphasis on radiotherapy, magnetic hyperthermia, and photothermal therapy (Table 5).

Radiotherapy is extensively employed in clinics for the treatment of cancer but the presence of tumor hypoxic microenvironments is responsible for degrading its therapeutic efficiency. Intending to reduce tumor hypoxia and enhance the efficacy of radioisotope therapy (RIT), Tao *et al.* developed PEG-modified rGO–MnO_2 nanocomposites (rGO–MnO_2–PEG). (Fig. 12) Intravenous injection of ^{131}I radiolabeled rGO–MnO_2–PEG into mice resulted in long-term blood circulation and considerable tumor accumulation. It is worth noting that in the presence of H_2O_2, MnO_2 nanoparticles are decomposed to Mn^{2+}, which could serve as a strong T_1-weighed contrast agent for MRI. The *in vitro* MR imaging of rGO–MnO_2–PEG nanocomposites has been examined at different concentrations of Mn^{2+}, at pH 7.4 and 5.8. The r_1 value at a pH of 5.8 (3.86 mM^{-1} s^{-1}) was found to be significantly higher than the r_1 value at a pH value of 7.4 (0.79 mM^{-1} s^{-1}).[113]

Hyperthermia, also known as green therapy, is extensively used as an adjuvant therapy with chemo and/or radiotherapy, leading to a significant improvement in the outcomes for cancer therapy. Recently, Kiamohammadi and co-workers proposed a novel strategy for exploiting the 5-Fu/SPION/NGO@PCL–LMWC as an MRI contrast agent and as a new platform for synergistic thermo-chemotherapy;[114] 5-Fu-loaded nanoparticles were injected into tumor-bearing mice. The targeted delivery was subsequently amplified using a magnetic field before being exposed to an alternating magnetic field (AMF). Magnetic Resonance Imaging helped to conveniently track the significant level of accumulation of 5-Fu loaded MNPs within the tumor site. The *in vitro* data revealed that the combination of 5-Fu-loaded nanoparticles and AMF hyperthermia dramatically lowered the cell plating efficiency. The results support the idea that the active targeting by an external magnetic field, after intravenously injecting the MNPs and exposing the tumor with the AMF, can be an efficient way to enhance the therapeutic efficiency.

Photothermal therapy (PTT) is a highly selective and minimally invasive treatment technique for cancer, employing nanoparticles capable of photoabsorption to generate heat under Near-infrared (NIR) irradiation, thereby causing thermal ablation of cancer cells. The growing use of graphene-based nanomaterials in PTT can be ascribed to their superior absorbance in the NIR range. Yang and co-workers prepared a graphene-based nanocomposite, RGO–IONP–PEG, with transverse relaxivity of 108.1 mM^{-1} s^{-1} at 3 T, for cancer theranostic applications. The nanocomposite was capable of *in vivo* triple modal photoacoustic tomography (PAT), fluorescence, and magnetic resonance (MR) tumor imaging. They carried out *in vivo* MR imaging guiding photothermal therapy (PTT) in tumor-bearing mice and could achieve highly efficient tumor ablation with a low laser power density.[81] Du, Liu, and co-workers successfully made a pioneering attempt in preparing a reduced graphene oxide anchoring iron oxide (RGI) whose surface charge is tunable, *via* a one-pot hydrothermal method.[82] They used polyethyleneimines (PEIs) of various molecular weights to obtain different positive charges on the surface and to control its stability. Owing to its positively charged surface, the RGI modified by 1.8 kDa

Table 5 Various graphene-based multifunctional nanocomposites with theranostic applications

S. No.	Nanomaterial	Type of potential MRI contrast agent	Relaxivity value (mM^{-1} s^{-1})	Therapeutic modality	Ref.
1.	GO/$MnFe_2O_4$/DOX	T_2	122	Photothermal therapy	115
2.	RGO–IONP–PEG	T_2	108.1	Photothermal therapy	81
3.	GO-IONP-PEG-DOX (GIPD)	T_1/T_2	—	Chemo-photothermal therapy	86
4.	5-Fu/SPION/NGO@PCL−LMWC	T_2	—	Magnetic hyperthermia	114
5.	GO/$BaGdF_5$/PEG	T_1	4.8	Photothermal therapy	116
6.	rGO–MnO_2–PEG	T_1	3.86	Radiotherapy	113
7.	nZVI/rGO@pDA	T_2	—	Photothermal therapy	117
8.	$RGI_{1.8k}$-ICG	T_2	—	Photothermal therapy	82
9.	NGO-SPION-PLGA-5-Fu	T_2	—	Photothermal therapy	118
10.	$CoFe_2O_4$/GO	T_2	92.7	Chemotherapy	103
11.	GO-IO-DOX	T_2	84	Hyperthermia, chemotherapy	119
12.	CAD-SPIONs@GO	T_1	3.17	Chemotherapy	120
13.	GQDs-Fe/Bi	T_2	62.34	Photothermal therapy (PTT)	121
14.	GO/$ZnFe_2O_4$/UCNPs	T_2	24.84	Phototherapy	122
15.	MNP/GO/chitosan	T_2	44.51	Chemotherapy	123
16.	GO-CD/Fe@C/DOX	T_2	9.37	Chemotherapy	124
17.	IUdR/NGO/SPION/PLGA	T_2	—	Photothermal therapy, chemotherapy	77
18.	GO-IONP-PEG	T_2	—	Photothermal therapy	125
19.	GO-IONP-Au-PEG	T_2	62.79	Photothermal therapy	107
20.	Magnetic graphene-based mesoporous silica (MGMS)	T_2	—	Chemo-photothermal therapy	109

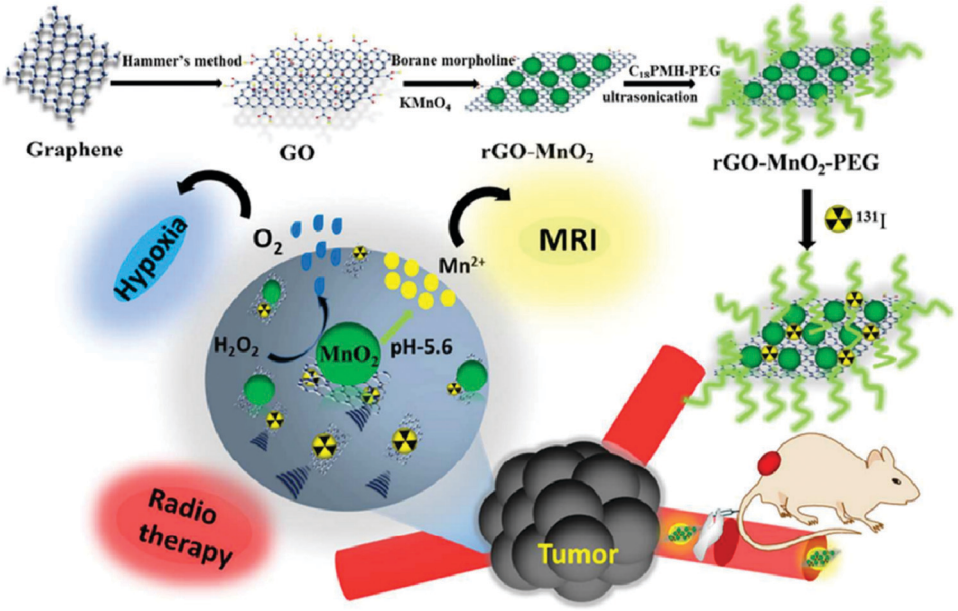

Fig. 12 Schematic illustration of the formation of ^{131}I-rGO–MnO_2–PEG nanocomposites for reducing tumor hypoxia and enhancing radioisotope therapy efficiency. Reprinted from ref. 113 Copyright 2018 Royal Society of Chemistry.

polyethyleneimine, $RGI_{1.8k}$, was found to be capable of effectively loading indocyanine green (ICG) and could serve as an excellent photothermal therapy (PTT) agent with high cellular internalization. Furthermore, the $RGI_{1.8k}$-ICG offered several advantages such as improved *in vivo* and *in vitro* cellular uptake capability, ablation of cancer cells with laser irradiation of low densities, *in vivo* infrared thermal imaging, and T_2-weighted magnetic resonance imaging. The GO-IONP composite developed by Li *et al.* displayed a photothermal effect, capable of destroying the thick shell of tumor tissue, hence rendering easy delivery of anticancer drugs into tumor cells[86] (Fig. 13).

6. Cytotoxicity and biocompatibility

Lower cytotoxicity and compatibility towards living tissues are two of the most important attributes of an MRI contrast agent, and these are the two aspects that set apart graphene-based NPs from other NPs. Various cytotoxicity studies have pointed out the minimal cytotoxicity of graphene-based magnetic nanoparticles.

Graphene oxide exhibits low cytotoxicity but the presence of GO could stimulate the complement activation by identifying the major biomarker molecules in plasma.[69] The toxicity can be further alleviated by surface modifications or coating with

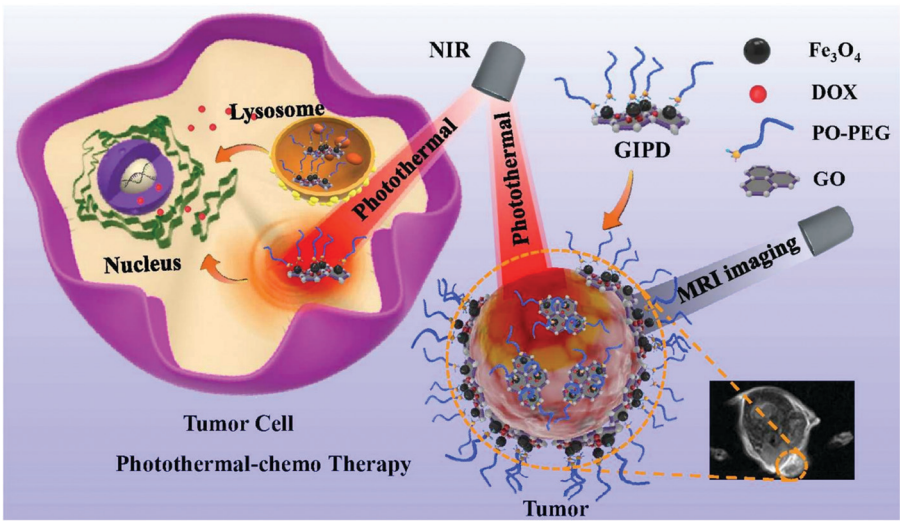

Fig. 13 Ultrasmall IONP-decorated graphene oxide (GO) nanohybrids present T_1/T_2 dual MRI imaging-guided photothermal-chemo combined anticancer theranostics efficacy. Reprinted from ref. 86 Copyright 2020 Royal Society of Chemistry.

biocompatible polymers such as polyethylene glycol (PEG), polyethyleneimine (PEI), and dextran.[69,85,126] Amino dextran (AMD) is one such derivative that has been extensively used due to its favorable biodegradability.[102] Amine-modified graphenes are found to be a safer substitute to other graphene derivatives, for biomedical applications.[127] Gd_2O_3–graphene oxide nanocomposites (GDO–GO NC) showed acceptable biocompatibility, making them potential T_1 contrast agents.[6] A methyl thiazolyl tetrazolium (MTT) assay was carried out using MCF-7 (human breast cancer cells) to analyze the cytotoxicity of the GO–$CoFe_2O_4$ nanocomposites wherein considerable biocompatibility was displayed towards the MCF-7 cell line.[45] Analysis of the MTT assay for GO–Fe_3O_4 composites showed that they were toxic to MCF-7 (Human breast cancer cells) but showed biocompatibility with normal cell lines (HaCaT).[46] No significant cytotoxicity effect was exhibited by Gd_2O_3/graphene quantum dot (GQD) nanocomposites toward both MCF-7 and NIH/3T3 (mouse embryonic fibroblasts) cell lines.[60] Zan *et al.* asserted that the unique hydrophilic structure of the Fe_3O_4/graphene nanocomposite renders it biocompatible, non-toxic, and colloidally stable in aqueous solutions.[79]

6.1 *In vitro* cytotoxicity

The aggregation state and surface charge of the nanomaterials are the most important factors that influence their *in vitro* cytotoxicity. In 2019, Alazmi *et al.* used a CCK-8 assay on HeLa cell lines to evaluate the cytotoxicity of rGOs with $CoFe_2O_4$ loading. As shown in Fig. 14, the cell viability was inversely proportional to the rGO concentration and the $CoFe_2O_4$–rGO hybrid systems exhibited low cytotoxicity, as expected.[59] An MTT assay performed on the HEK293 human kidney line suggested that GO-PEG-β-FeOOH has a negligible *in vitro* cytotoxicity.[74] Moreover, the biodegradability of β-FeOOH is desirable along with its ability to get into cancer cells easily thus rendering it a good *in vivo* imaging contrast agent.[74]

The cytotoxicity test carried out in HCT-116 cell lines using a standard MTT assay test revealed that the nanocomposite, GO-*g*-PCA/γ-Fe_2O, prepared by Torkashvand and his team, exhibited good biocompatibility and very low cytotoxicity even at high concentrations.[50] The biodegradability studies of PLGA (poly lactic-*co*-glycolic acid) affirm its potential as a good nanocarrier.[77] Nkansah *et al.* studied the biodegradability of SPION and concluded that around 100 days were necessary to remove them.[128] NGO/SPION/PLGA exhibited no notable cytotoxicity. Moreover, the nanocomposite showed remarkable cell viability even at high concentrations.[77]

6.2 *In vivo* cytotoxicity

Only a limited amount of exploration has been performed to date to study the *in vivo* cytotoxicity effect of graphene-based nanomaterials;[58] a study of polyethylene glycosylated GO showed no palpable toxicity.[69] *In vivo* analysis showed that the water-soluble, and colloidally-stable, Fe_3O_4/G nanocomposite exhibited excellent biocompatibility and could be cleared from the body through metabolic processes.[79]Although these observations hint towards the good biocompatibility of these MRI contrast agents, more confirmative pieces of evidence are required from thorough *in vivo* cytotoxicity studies to draw any definitive conclusions about their potential as MRI contrast agents.

7. Concluding remarks and future outlook

Magnetic resonance imaging (MRI) is garnering escalating interest in clinical diagnosis. Developments in recent years have been focused on the design of MRI contrast agents. In view of this background, our review will be useful in the field of clinical diagnosis using MRI, as the majority of the recent research work has been performed in the field of contrast-enhanced MRI, deploying graphene-decorated magnetic nanocarriers as contrast agents. Today, contrast-enhanced MRI is a valuable technique for multiple indications in many body parts and the coming decade is expected to provide further major advances in diagnostic MRI. Graphene-based materials (GBMs)

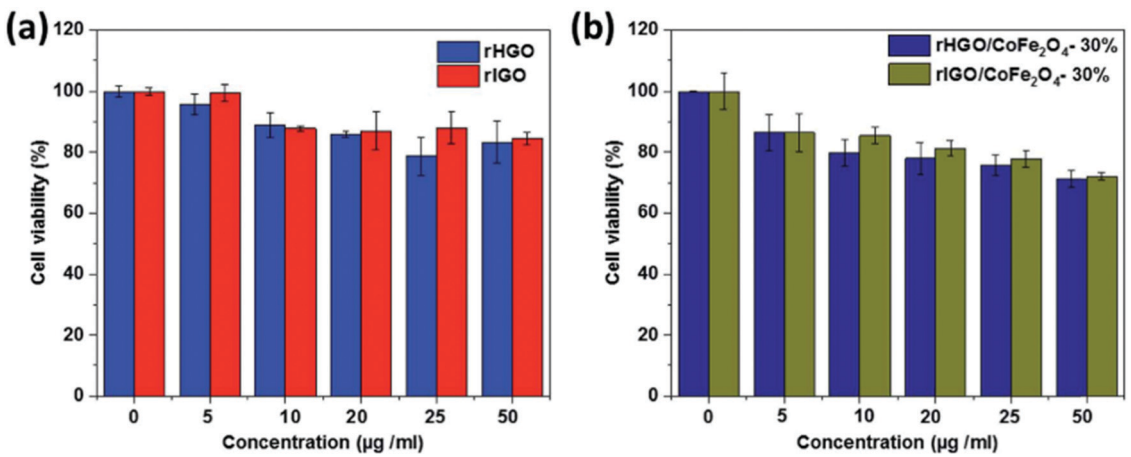

Fig. 14 Viability of HeLa cells at various concentrations of (a) rHGO and rIGO and (b) rHGO/$CoFe_2O_4$ and rIGO/$CoFe_2O_4$. Reprinted from ref. 59 Copyright 2019 Royal Society of Chemistry.

such as graphene oxide (GO) and reduced graphene oxide (rGO), due to their characteristic structure and physicochemical properties, have captured broad research attention. The high dispersibility, specific target ability, capacity for efficient loading of MNPs, biocompatibility, and low toxicity are the main attributes of GBMs which make them promising candidates for imaging applications. Their combination with MNPs generates excellent magnetic hybrids which can also function as multifunctional systems. Loading of magnetic contrast agents on the surface of GO decreases their release rate and increases their proton relaxivity value to a great extent. Anchoring heavy metal ion contrast agents on GO may alleviate their toxicity due to the decreased release rate. However, this field is still far away from clinical applications and Gd-based contrast agents remain the most commonly used materials in clinical applications. This is because they are less toxic and are easily removed from the body. Improving the relaxivity of T_2 contrast agents is a more challenging task for researchers because of their lower signal enhancing ability as compared to T_1 contrast agents. Although graphene-decorated magnetic nanomaterials have been extensively studied, an even brighter future is expected in this field.

Conflicts of interest

The authors declare no conflict of interest, financial or otherwise.

References

1 Y. Yang, A. M. Asiri, Z. Tang, D. Du and Y. Lin, *Mater. Today*, 2013, **16**, 365–373.
2 A. Pohlmann, K. Cantow, J. Hentschel, K. Arakelyan, M. Ladwig, B. Flemming, U. Hoff, P. B. Persson, E. Seeliger and T. Niendorf, *Acta Physiol.*, 2013, **207**, 673–689.
3 Y. Gao, *J. Funct. Biomater.*, 2018, **9**, 1–15.
4 E. J. Werner, A. Datta, C. J. Jocher and K. N. Raymond, *Angew. Chem., Int. Ed.*, 2008, **47**, 8568–8580.
5 H. Bin Na and T. Hyeon, *J. Mater. Chem.*, 2009, **19**, 6267–6273.
6 F. Wang, E. Peng, B. Zheng, S. F. Y. Li and J. M. Xue, *J. Phys. Chem. C*, 2015, **119**, 23735–23742.
7 S. Iravani and R. S. Varma, *Environ. Chem. Lett.*, 2020, **18**, 703–727.
8 M. Fiorillo, A. F. Verre, M. Iliut, M. Peiris-Pagés, B. Ozsvari, R. Gandara, A. R. Cappello, F. Sotgia, A. Vijayaraghavan and M. P. Lisanti, *Oncotarget*, 2015, **6**, 3553–3562.
9 C. Wang, J. Li, C. Amatore, Y. Chen, H. Jiang and X.-M. Wang, *Angew. Chemie*, 2011, **123**, 11848–11852.
10 F. M. Tonelli, V. A. Goulart, K. N. Gomes, M. S. Ladeira, A. K. Santos, E. Lorençon, L. O. Ladeira and R. R. Resende, *Nanomedicine*, 2015, **10**, 2423–2450.
11 B. Zhang, Y. Wang and G. Zhai, *Mater. Sci. Eng., C*, 2016, **61**, 953–964.
12 J. Lin, Y. Huang and P. Huang, *Graphene-Based Nanomaterials in Bioimaging*, Elsevier Inc., 2018.
13 T. P. Dasari Shareena, D. McShan, A. K. Dasmahapatra and P. B. Tchounwou, *Nano-Micro Lett.*, 2018, **10**, 1–34.
14 X. Ren, X. Jing, L. Liu, L. Guo, M. Zhang and Y. Li, *RSC Adv.*, 2014, **4**, 53987–53992.
15 M. Llenas, S. Sandoval, P. M. Costa, J. Oró-Solé, S. Lope-Piedrafita, B. Ballesteros, K. T. Al-Jamal and G. Tobias, *Nanomaterials*, 2019, **9**(10), 1364.
16 K. Zhang, J. M. Suh, T. H. Lee, J. H. Cha, J. W. Choi, H. W. Jang, R. S. Varma and M. Shokouhimehr, *Nano Converge.*, 2019, **6**, 0–6.
17 V. V. T. Padil, S. Wacławek, M. Černík and R. S. Varma, *Biotechnol. Adv.*, 2018, **36**, 1984–2016.
18 S. Iravani and R. S. Varma, *Green Chem.*, 2020, **22**, 2643–2661.
19 N. Rabiee, M. Bagherzadeh, A. M. Ghadiri, M. Kiani, Y. Fatahi, M. Tavakolizadeh, A. Pourjavadi, M. Jouyandeh, M. R. Saeb, M. Mozafari, M. Shokouhimehr and R. S. Varma, *ACS Sustainable Chem. Eng.*, 2021, **9**, 8706–8720.
20 E. N. Zare, T. Agarwal, A. Zarepour, F. Pinelli, A. Zarrabi, F. Rossi, M. Ashrafizadeh, A. Maleki, M. A. Shahbazi, T. K. Maiti, R. S. Varma, F. R. Tay, M. R. Hamblin, V. Mattoli and P. Makvandi, *Appl. Mater. Today*, 2021, **24**, 101117.
21 P. Makvandi, A. Zarepour, X. Zheng, T. Agarwal, M. Ghomi, R. Sartorius, E. N. Zare, A. Zarrabi, A. Wu, T. K. Maiti, B. R. Smith, R. S. Varma, F. R. Tay and V. Mattoli, *Appl. Mater. Today*, 2021, **24**, 101107.
22 M. Ashrafizadeh, M. Delfi, F. Hashemi, A. Zabolian, H. Saleki, M. Bagherian, N. Azami, M. V. Farahani, S. O. Sharifzadeh, S. Hamzehlou, K. Hushmandi, P. Makvandi, A. Zarrabi, M. R. Hamblin and R. S. Varma, *Carbohydr. Polym.*, 2021, **260**, 117809.
23 S. Kumar, A. Mongia, S. Gulati, P. Singh, A. Diwan and S. Shukla, *Cancer Treat. Res. Commun.*, 2020, **25**, 100258.
24 S. Kumar, A. Diwan, P. Singh, S. Gulati, D. Choudhary, A. Mongia, S. Shukla and A. Gupta, *RSC Adv.*, 2019, **9**, 23894–23907.
25 S. Gulati, P. Singh, A. Diwan, A. Mongia and S. Kumar, *RSC Med. Chem.*, 2020, **11**, 1252–1266.
26 S. Gulati, S. Kumar, P. Singh, A. Diwan and A. Mongia, *Handb. Polym. Ceram. Nanotechnol.*, 2021, 811–838.
27 S. S. Nanda, G. C. Papaefthymiou and D. K. Yi, *Crit. Rev. Solid State Mater. Sci.*, 2015, **40**, 291–315.
28 A. H. Castro Neto, F. Guinea, N. M. R. Peres, K. S. Novoselov and A. K. Geim, *Rev. Mod. Phys.*, 2009, **81**, 109–162.
29 H. Shen, L. Zhang, M. Liu and Z. Zhang, *Theranostics*, 2012, **2**, 283–294.
30 K. S. Novoselov, A. K. Geim, S. V. Morozov, D. Jiang, Y. Zhang, S. V. Dubonos, I. V. Grigorieva and A. A. Firsov, *Science*, 2004, **306**, 666–669.
31 K. Zhang, L. L. Zhang, X. S. Zhao and J. Wu, *Chem. Mater.*, 2010, **22**, 1392–1401.
32 C. N. R. Rao, A. K. Sood, K. S. Subrahmanyam and A. Govindaraj, *Angew. Chem., Int. Ed.*, 2009, **48**, 7752–7777.

33 A. A. Balandin, S. Ghosh, W. Bao, I. Calizo, D. Teweldebrhan, F. Miao and C. N. Lau, *Nano Lett.*, 2008, **8**, 902–907.
34 S. Latil and L. Henrard, *Phys. Rev. Lett.*, 2006, **97**, 1–4.
35 M. Khan, M. N. Tahir, S. F. Adil, H. U. Khan, M. R. H. Siddiqui, A. A. Al-Warthan and W. Tremel, *J. Mater. Chem. A*, 2015, **3**, 18753–18808.
36 B. Jaleh, E. Zare, S. Azizian, O. Qanati, M. Nasrollahzadeh and R. S. Varma, *J. Inorg. Organomet. Polym. Mater.*, 2020, **30**, 2213–2223.
37 G. Shim, M. G. Kim, J. Y. Park and Y. K. Oh, *Adv. Drug Delivery Rev.*, 2016, **105**, 205–227.
38 Y. Ioni, E. Buslaeva and S. Gubin, *Mater. Today Proc.*, 2016, **3**, S209–S213.
39 A. Goswami, A. K. Rathi, C. Aparicio, O. Tomanec, M. Petr, R. Pocklanova, M. B. Gawande, R. S. Varma and R. Zboril, *ACS Appl. Mater. Interfaces*, 2017, **9**, 2815–2824.
40 A. Venkateshaiah, D. Silvestri, R. K. Ramakrishnan, S. Wacławek, V. V. T. Padil, M. Černík and R. S. Varma, *Molecules*, 2019, **24**, 1–11.
41 G. Wang, G. Chen, Z. Wei, X. Dong and M. Qi, *Mater. Chem. Phys.*, 2013, **141**, 997–1004.
42 N. Alegret, A. Criado and M. Prato, *Curr. Med. Chem.*, 2017, 529–536.
43 W. S. Hummers and R. E. Offeman, *J. Am. Chem. Soc.*, 1957, **208**, 1937.
44 M. J. Yoo and H. B. Park, *Carbon N. Y.*, 2019, **141**, 515–522.
45 N. Venkatesha, P. Poojar, R. Ashwini, Y. Qurishi, S. Geethanath and C. Srivastava, *RSC Adv.*, 2016, **6**, 17423–17429.
46 N. Venkatesha, P. Poojar, Y. Qurishi, S. Geethanath and C. Srivastava, *J. Appl. Phys.*, 2015, **117**, 154702.
47 N. Torkashvand and N. Sarlak, *Colloids Surf., B*, 2020, **185**, 110555.
48 N. Sarlak and T. J. Meyer, *J. Mol. Liq.*, 2017, **243**, 654–663.
49 Y. Xu, K. Sheng, C. Li and G. Shi, *J. Mater. Chem.*, 2011, **21**, 7376–7380.
50 N. Torkashvand and N. Sarlak, *J. Mol. Liq.*, 2019, **291**, 111286.
51 S. D. Senol, A. Guler, C. Boyraz and L. Arda, *J. Supercond. Nov. Magn.*, 2019, **32**, 2781–2786.
52 S. Bai and X. Shen, *RSC Adv.*, 2012, **2**, 64–98.
53 M. Ge, C. Cao, J. Huang, S. Li, Z. Chen, K. Q. Zhang, S. S. Al-Deyab and Y. Lai, *J. Mater. Chem. A*, 2016, **4**, 6772–6801.
54 Y. Wang, J. Yu, W. Xiao and Q. Li, *J. Mater. Chem. A*, 2014, **2**, 3847–3855.
55 J. Livage, *Materials*, 2010, **3**, 4175–4195.
56 Y. X. Gan, A. H. Jayatissa, Z. Yu, X. Chen and M. Li, *J. Nanomater.*, 2020, **2020**, 8917013.
57 P. T. Yin, S. Shah, M. Chhowalla and K. B. Lee, *Chem. Rev.*, 2015, **115**, 2483–2531.
58 J. M. Shen, G. Huang, X. Zhou, J. Zou, Y. Yang, Y. F. Chen and S. K. Men, *RSC Adv.*, 2014, **4**, 50464–50477.
59 A. Alazmi, V. Singaravelu, N. M. Batra, J. Smajic, M. Alyami, N. M. Khashab and P. M. F. J. Costa, *RSC Adv.*, 2019, **9**, 6299–6309.
60 F. H. Wang, K. Bae, Z. W. Huang and J. M. Xue, *Nanoscale*, 2018, **10**, 5642–5649.
61 J. Lohrke, T. Frenzel, J. Endrikat, F. C. Alves, T. M. Grist, M. Law, J. M. Lee, T. Leiner, K. C. Li, K. Nikolaou, M. R. Prince, H. H. Schild, J. C. Weinreb, K. Yoshikawa and H. Pietsch, *Adv. Ther.*, 2016, **33**, 1–28.
62 Y. D. Xiao, R. Paudel, J. Liu, C. Ma, Z. S. Zhang and S. K. Zhou, *Int. J. Mol. Med.*, 2016, **38**, 1319–1326.
63 C. Burtea, S. Laurent, L. Vander Elst and R. N. Muller, *Handb. Exp. Pharmacol.*, 2008, **185**, 135–165.
64 I. Fernández-Barahona, M. Muñoz-Hernando, J. Ruiz-Cabello, F. Herranz and J. Pellico, *Inorganics*, 2020, **8**, 1–22.
65 X. Yin, S. E. Russek, G. Zabow, F. Sun, J. Mohapatra, K. E. Keenan, M. A. Boss, H. Zeng, J. P. Liu, A. Viert, S. H. Liou and J. Moreland, *Sci. Rep.*, 2018, **8**, 1–10.
66 M. Wu, Q. Meng, Y. Chen, P. Xu, S. Zhang, Y. Li, L. Zhang, M. Wang, H. Yao and J. Shi, *Adv. Funct. Mater.*, 2014, **24**, 4273–4283.
67 J. Estelrich, M. J. Sánchez-Martín and M. A. Busquets, *Int. J. Nanomed.*, 2015, **10**, 1727–1741.
68 U. I. Tromsdorf, N. C. Bigall, M. G. Kaul, O. T. Bruns, M. S. Nikolic, B. Mollwitz, R. A. Sperling, R. Reimer, H. Hohenberg, W. J. Parak, S. Förster, U. Beisiegel, G. Adam and H. Weller, *Nano Lett.*, 2007, **7**, 2422–2427.
69 M. Zhang, Y. Cao, Y. Chong, Y. Ma, H. Zhang, Z. Deng, C. Hu and Z. Zhang, *ACS Appl. Mater. Interfaces*, 2013, **5**, 13325–13332.
70 M. Zhang, X. Liu, J. Huang, L. Wang, H. Shen, Y. Luo, Z. Li, H. Zhang, Z. Deng and Z. Zhang, *Nanomed. Nanotechnol., Biol. Med.*, 2018, **14**, 2475–2483.
71 S. M. Chowdhury, S. Kanakia, J. D. Toussaint, M. D. Frame, A. M. Dewar, K. R. Shroyer, W. Moore and B. Sitharaman, *Sci. Rep.*, 2013, **3**, 2–4.
72 S. Kanakia, J. D. Toussaint, S. Mullick Chowdhury, T. Tembulkar, S. Lee, Y. P. Jiang, R. Z. Lin, K. R. Shroyer, W. Moore and B. Sitharaman, *Biomaterials*, 2014, **35**, 7022–7031.
73 S. Kanakia, J. Toussaint, D. M. Hoang, S. M. Chowdhury, S. Lee, K. R. Shroyer, W. Moore, Y. Z. Wadghiri and B. Sitharaman, *Sci. Rep.*, 2015, **5**, 1–12.
74 M. L. Chen, L. M. Shen, S. Chen, H. Wang, X. W. Chen and J. H. Wang, *J. Mater. Chem. B*, 2013, **1**, 2582–2589.
75 D. O. Idisi, J. A. Oke, S. Sarma, S. J. Moloi, S. C. Ray, W. F. Pong and A. M. Strydom, *J. Appl. Phys.*, 2019, **126**, 035301.
76 E. Peng, F. Wang, S. Tan, B. Zheng, S. F. Y. Li and J. M. Xue, *J. Mater. Chem. B*, 2015, **3**, 5678–5682.
77 S. Shirvalilou, S. Khoei, S. Khoee, N. J. Raoufi, M. R. Karimi and A. Shakeri-Zadeh, *Chem. – Biol. Interact.*, 2018, **295**, 97–108.
78 R. Gonzalez-Rodriguez, E. Campbell and A. Naumov, *PLoS One*, 2019, **14**, 1–18.
79 P. Zan, C. Yang, H. Sun, L. Zhao, Z. Lv and Y. He, *Colloids Surf., B*, 2016, **145**, 208–216.
80 E. Peng, E. S. G. Choo, P. Chandrasekharan, C. T. Yang, J. Ding, K. H. Chuang and J. M. Xue, *Small*, 2012, **8**, 3620–3630.
81 K. Yang, L. Hu, X. Ma, S. Ye, L. Cheng, X. Shi, C. Li, Y. Li and Z. Liu, *Adv. Mater.*, 2012, **24**, 1868–1872.

82 B. Du, J. Liu, G. Ding, X. Han, D. Li, E. Wang and J. Wang, *Nano Res.*, 2017, **10**, 2280–2295.
83 C. Zhou, H. Wu, M. Wang, C. Huang, D. Yang and N. Jia, *Mater. Sci. Eng., C*, 2017, **78**, 817–825.
84 M. Razaghi, A. Ramazani, M. Khoobi, T. Mortezazadeh, E. A. Aksoy and T. T. Küçükkılınç, *J. Drug Delivery Sci. Technol.*, 2020, **60**, 101967.
85 L. Cheng, K. Yang, M. Shao, X. Lu and Z. Liu, *Nanomedicine*, 2011, **6**, 1327–1340.
86 Y. Li, L. Zheng, L. Xiao, L. Wang, J. Cui, D. Sha and C. Liu, *Biomater. Sci.*, 2020, **8**, 6375–6386.
87 S. Sadighian, N. Bayat, S. Najaflou, M. Kermanian and M. Hamidi, *ChemistrySelect*, 2021, **6**, 2862–2868.
88 M. S. Usman, M. Z. Hussein, A. U. Kura, S. Fakurazi, M. J. Masarudin and F. F. Ahmad Saad, *Mater. Chem. Phys.*, 2020, **240**, 122232.
89 Y. Bao, J. A. Sherwood and Z. Sun, *J. Mater. Chem. C*, 2018, **6**, 1280–1290.
90 J. M. Idée, M. Port, A. Dencausse, E. Lancelot and C. Corot, *Radiol. Clin. North Am.*, 2009, **47**, 855–869.
91 H. S. Thomsen, S. K. Morcos, T. Almén, M. F. Bellin, M. Bertolotto, G. Bongartz, O. Clement, P. Leander, G. Heinz-Peer, P. Reimer, F. Stacul, A. Van Der Molen and J. A. Webb, *Eur. Radiol.*, 2013, **23**, 307–318.
92 Y. Xiang, N. Li, L. Guo, H. Wang, H. Sun, R. Li, L. Ma, Y. Qi, J. Zhan and D. Yu, *Carbon N. Y.*, 2018, **136**, 113–124.
93 J. Wahsner, E. M. Gale, A. Rodríguez-Rodríguez and P. Caravan, *Chem. Rev.*, 2019, **119**, 957–1057.
94 M. Rogosnitzky and S. Branch, *Biometals*, 2016, **29**, 365–376.
95 M. Perazella, *Curr. Drug Saf.*, 2008, **3**, 67–75.
96 L. Pasquini, A. Napolitano, E. Visconti, D. Longo, A. Romano, P. Tomà and M. C. R. Espagnet, *CNS Drugs*, 2018, **32**, 229–240.
97 H. K. Kim, G. H. Lee and Y. Chang, *Future Med. Chem.*, 2018, **10**, 639–661.
98 J. Pellico, C. M. Ellis and J. J. Davis, *Contrast Media Mol. Imaging*, 2019, **2019**, 1845637.
99 J. M. Yoo, J. H. Kang and B. H. Hong, *Chem. Soc. Rev.*, 2015, **44**, 4835–4852.
100 S. Kanakia, J. D. Toussaint, S. Mullick Chowdhury, G. Lalwani, T. Tembulkar, T. Button, K. R. Shroyer, W. Moore and B. Sitharaman, *Int. J. Nanomed.*, 2013, **8**, 2821–2833.
101 C. Rümenapp, B. Gleich and A. Haase, *Pharm. Res.*, 2012, **29**, 1165–1179.
102 W. Chen, P. Yi, Y. Zhang, L. Zhang, Z. Deng and Z. Zhang, *ACS Appl. Mater. Interfaces*, 2011, **3**, 4085–4091.
103 G. Wang, Y. Ma, Z. Wei and M. Qi, *Chem. Eng. J.*, 2016, **289**, 150–160.
104 H. Ersoy and F. J. Rybicki, *J. Magn. Reson. Imaging*, 2007, **26**, 1190–1197.
105 Z. Zhou and Z. R. Lu, *Wiley Interdiscip. Rev.: Nanomed. Nanobiotechnol.*, 2013, **5**, 1–18.
106 X. Cai, Q. Zhu, Y. Zeng, Q. Zeng, X. Chen and Y. Zhan, *Int. J. Nanomed.*, 2019, **14**, 8321–8344.
107 X. Shi, H. Gong, Y. Li, C. Wang, L. Cheng and Z. Liu, *Biomaterials*, 2013, **34**, 4786–4793.
108 A. J. Shen, D. L. Li, X. J. Cai, C. Y. Dong, H. Q. Dong, H. Y. Wen, G. H. Dai, P. J. Wang and Y. Y. Li, *J. Biomed. Mater. Res., Part A*, 2012, **100 A**, 2499–2506.
109 Y. Wang, R. Huang, G. Liang, Z. Zhang, P. Zhang, S. Yu and J. Kong, *Small*, 2014, **10**, 109–116.
110 D. Li, M. Deng, Z. Yu, W. Liu, G. Zhou, W. Li, X. Wang, D. P. Yang and W. Zhang, *ACS Biomater. Sci. Eng.*, 2018, **4**, 2143–2154.
111 A. Madni, S. Noreen, I. Maqbool, F. Rehman, A. Batool, P. M. Kashif, M. Rehman, N. Tahir and M. I. Khan, *J. Drug Target.*, 2018, **26**, 858–883.
112 S. Song, H. Shen, Y. Wang, X. Chu, J. Xie, N. Zhou and J. Shen, *Colloids Surf., B*, 2020, **185**, 110596.
113 Y. Tao, L. Zhu, Y. Zhao, X. Yi, L. Zhu, F. Ge, X. Mou, L. Chen, L. Sun and K. Yang, *Nanoscale*, 2018, **10**, 5114–5123.
114 L. Kiamohammadi, L. Asadi, S. Shirvalilou, S. Khoei, S. Khoee, M. Soleymani and S. E. Minaei, *ACS Omega*, 2021, **6**, 20192–20204.
115 Y. Yang, H. Shi, Y. Wang, B. Shi, L. Guo, D. Wu, S. Yang and H. Wu, *J. Biomater. Appl.*, 2016, **30**, 810–822.
116 H. Zhang, H. Wu, J. Wang, Y. Yang, D. Wu, Y. Zhang, Y. Zhang, Z. Zhou and S. Yang, *Biomaterials*, 2015, **42**, 66–77.
117 C. H. Lin, Y. C. Chen and P. I. Huang, *Nanomaterials*, 2020, **10**, 1–13.
118 A. Mohammadi Gazestani, S. Khoei, S. Khoee, S. Emamgholizadeh Minaei and M. Motevalian, *Artif. Cells, Nanomed., Biotechnol.*, 2018, **46**, 25–33.
119 A. Ramachandra Kurup Sasikala, R. G. Thomas, A. R. Unnithan, B. Saravanakumar, Y. Y. Jeong, C. H. Park and C. S. Kim, *Sci. Rep.*, 2016, **6**, 1–14.
120 Y. Luo, Y. Tang, T. Liu, Q. Chen, X. Zhou, N. Wang, M. Ma, Y. Cheng and H. Chen, *Chem. Commun.*, 2019, **55**, 1963–1966.
121 S. Badrigilan, B. Shaabani, N. Gharehaghaji and A. Mesbahi, *Photodiagnosis Photodyn. Ther.*, 2019, **25**, 504–514.
122 H. Bi, F. He, Y. Dai, J. Xu, Y. Dong, D. Yang, S. Gai, L. Li, C. Li and P. Yang, *Inorg. Chem.*, 2018, **57**, 9988–9998.
123 M. S. Baktash, A. Zarrabi, E. Avazverdi and N. M. Reis, *J. Mol. Liq.*, 2021, **322**, 114515.
124 Y. H. Hsu, H. L. Hsieh, G. Viswanathan, S. H. Voon, C. S. Kue, W. S. Saw, C. H. Yeong, C. A. Azlan, T. Imae, L. V. Kiew, H. B. Lee and L. Y. Chung, *J. Nanoparticle Res.*, 2017, **19**, 359.
125 S. Wang, Q. Zhang, X. F. Luo, J. Li, H. He, F. Yang, Y. Di, C. Jin, X. G. Jiang, S. Shen and D. L. Fu, *Biomaterials*, 2014, **35**, 9473–9483.
126 A. M. Jastrzębska, P. Kurtycz and A. R. Olszyna, *J. Nanoparticle Res.*, 2012, **14**, 1320.
127 S. K. Singh, M. K. Singh, P. P. Kulkarni, V. K. Sonkar, J. J. A. Grácio and D. Dash, *ACS Nano*, 2012, **6**, 2731–2740.
128 M. K. Nkansah, D. Thakral and E. M. Shapiro, *Magn. Reson. Med.*, 2011, **65**, 1776–1785.